Electron Tomography of Chromosome Structure

Peter Engelhardt

in
Encyclopedia of Analytical Chemistry
R.A. Meyers (Ed.)
pp. 4948–4984

Electron Tomography of Chromosome Structure

Peter Engelhardt
Haartman Institute, University of Helsinki, Helsinki, Finland

1 Introduction **2**
1.1 Chromosome Structure 2
1.2 Electron Tomography Compared with Earlier Methods 9
2 Preparation Steps for Chromosomes **9**
2.1 General 9
2.2 Chromosome Isolation and Whole Mounts 10
2.3 Pretreatments: Salt Extraction and Enzyme Digestions 12
2.4 Fixation of Chromosomes 13
3 Preservation Methods for Three-dimensional Reconstructions **15**
3.1 Critical-point Drying 15
3.2 Drying from *tert*-Butanol 16
3.3 Freeze-drying 16
3.4 Cryo-electron Tomography 17
3.5 Section Preparations 17
4 Data Collection **18**
4.1 Recording of Tilt Series 18
4.2 Manual Recording 19
4.3 Digitalization of Photographic Negatives 19
4.4 Automatic Recording 20
5 Electron Tomography Methods **21**
5.1 Alignment of Tilt Series 21
5.2 Reconstruction Methods 22
5.3 Weighted Back-projection Method 22
5.4 Maximum Entropy Method 22
5.5 Dual-axis Tilting Method 23
6 Rendering of Reconstructed Chromosomes **24**
6.1 Visualization of Three-dimensional Reconstructions 24
6.2 Producing Stereo Animations from Three-dimensional Volumes 27
6.3 Computer-aided Virtual Environment 28
7 Immunoelectron Tomography **29**
8 In Situ Hybridization Electron Tomography **31**
9 Hard Copies, Production of Solid Three-dimensional Models **32**
10 Method Development **32**
Acknowledgments **32**
Abbreviations and Acronyms **33**
Related Articles **33**
References **34**

Three-dimensional (3-D) structures at the molecular level of chromosomes and other cell structures are far beyond the reach of ordinary or confocal (3-D) light microscopy (LM). The electron tomography method (ETM), i.e. transmission electron microscopy (TEM) tomography, is able to provide methods of 3-D reconstruction of macromolecular assemblies, providing insights into the qualitative and quantitative spatial comprehension of macromolecular structures. ETM is a powerful method for developing reliable immunoelectron tomography (IET) and in situ hybridization analysis at the molecular level.

With ETM the data are collected with TEM by taking tilt series, i.e. projection images from different viewing angles over the object. By combining such projections taken over a sufficient angular range (from 0 to $\pm 60^{\circ}$ manually, e.g. in 3° increments), a wholly transparent 3-D representation of the object is recovered with necessary details. This requires the use of suitable computational methods.

Automatic single-axis tilt-series data registration is possible today that will not only allow the collection of data with increments as small as 1°, for high-resolution reconstructions of bulky whole mounts, but will also protect the specimen from electron beam damage (dose reduced by a factor of 10–100). Only automation of ETM procedures makes it possible to collect tilt series of cryo-electron microscopy (EM) preparations of unfixed and unstained preparations in vitrified ice, i.e. fully hydrated samples close to the native state.

Novel methods and tools for electron tomography are available that have been developed in different laboratories. Our electron tomography programs are automated to a high degree and therefore very fast and easy to use, in comparison with other program kits that are available. Specifically, our arsenal includes advanced tomography procedures based on the maximum entropy method (MEM) (e.g. 16-bit gray-scale MEM).

A collection of preparative methods for preserving whole-mounted chromosomes and cells for ETM studies has been developed. Examples of 3-D reconstructions of human chromosomes are shown at high resolution (3–15 nm).

It is considered that ETM allows 3-D reconstructions, depending on the thickness of the preparation, with a

Encyclopedia of Analytical Chemistry
R.A. Meyers (Ed.)

resolution in the range 2.5–8.5 nm. In this respect, some success was recently made as we were able to detect nanoprobes (1.4-nm immunogold markers) with the IET methods developed.

ETM of chromosomes involving localized genes with in situ hybridization and gold-labeling techniques is possible and would allow chromosome mapping in a 3-D configuration with molecular resolution much more accurately than any standard EM method which are affected by superimposing gold labels with their accompanying structures.

Concerning the structure and folding of the DNA in chromosomes, it is important to note that the linear sequence of bases in DNA is accompanied by higher level organizations, composed of loops, twists and folds in the long DNA chain, and, significantly, by DNA–protein interactions, e.g. nucleosomes, supranucleosomes, together with telomerase, topoisomerases and the new scaffold proteins [structural maintenance of chromosomes (SMC) family] recently described. These so-called 'higher order structures' are certainly very much involved in the regulation of gene expression in chromosomes. Further, it is easy to realize that genes distantly located in the linear sequence map could in fact be topologically associated when DNA is folded in chromosomes, and thus mutually regulated. Sequencing of the genomes does not include and cannot reveal higher order structures. It is only with ETM that genome maps can be brought in relation to 3-D molecular configurations, and it can be refined by combination with in situ hybridization to localize gene sequences and with IET to identify chromosomal proteins.

1 INTRODUCTION

1.1 Chromosome Structure

Higher order chromosome structure is an enigmatic and challenging problem. It is more than 100 years since the word chromosome first appeared in the literature,[1] and almost 50 years since the principle of the DNA structure was established.[2] The discovery of DNA structure was a turning point in biology and initiated the rapid development of molecular biology. We have been treated to detailed descriptions of various biological structures at the molecular level and various roles have been attributed to DNA. As for DNA, the overall principle of replication is clear, but many details even of replication have turned out to be uncompromisingly complex.[3] In addition, the organization of DNA and the regulation of its function in interphase nuclei and its condensation into metaphase chromosomes at mitosis remain a distressing tangle in cell biology.

Difficulties in solving chromosome structure largely stem from the huge amount of DNA wrapped into chromosomes. Yet the packing and organization of the DNA in many phages and viruses with basically less DNA are also unclear.[4] The length of DNA per diploid human somatic nuclei (diameter about 5–10 μm) is about 1.8 m. In mitosis twice as much is arranged into 46 chromosomes with a total length of about 200 μm. Consequently, the compaction proportion of the DNA in chromosomes is about $10^4 : 1$.[5]

In addition, the length and thickness of the chromosomes change dynamically when chromosomes condense in mitosis. Related changes are observed in meiosis, although the chromosomes are more attenuated and delicate, forming the so-called synaptonemal complexes when chromosomes pair up. In mitosis, early prophase chromosomes appear as long strands that reach full compression at metaphase. After mitosis, the chromosomes revert to their diffuse interphase form. In the interphase nucleus, chromosome positions tend to be conserved in their anaphase–telophase configurations. In this orientation, called the Rabl orientation,[6] centromeres and telomeres occupy opposite regions of the nucleus. The chromosomes somehow rearrange themselves before the next division. Regions of interphase chromosomes, in yeast and *Drosophila*, have recently been shown to be in Brownian motion limited to a subvolume no more than 1% of the total nuclear volume of living cells.[7]

What regulates, causes and lies behind the interphase chromosome movements and prophase contraction at the molecular level is not known, but such movements may be caused by proteins analogous to the contractile proteins of the cytoskeleton. Microtubules have not been observed, in higher eukaryotes, inside nuclei as long as the nuclear envelope (NE) remains intact. In lower eukaryotes, e.g. in yeast cells, bundles of microtubules are detected inside cell nucleus, at mitosis, as the NE remains intact in the budding. Bundles of striated microfilaments[8] have been described in meiosis along the lateral elements of the synaptonemal complex (SC) and shown by immunological methods[9] to react like actin, myosin and tubulin. The actual involvement in meiosis of these and many other immunologically indicated proteins is still controversial.[9] It should be noted that the above-mentioned restricted Brownian motion of chromosome regions has been shown to be inhibited only by the microtubule-depolymerizing agent nocodazole[7] and not by sodium azide, which is known to stop ATPase-driven processes.

In recent years, new groups of proteins have been isolated and shown to participate in chromosome contraction (the SMC family of proteins),[10] sister chromatid cohesion apparatus (cohesin complex) and sister chromatid separation (separins that destroy cohesion).[11]

In the folding of the chromosomes, different levels can be distinguished. Remarkably, there is a better understanding of how the DNA is organized in the chromosomes at the molecular level than at the gross chromosome level. This discrepancy may partly be due to the fact that chromosomes are too small for detailed studies at the LM level and too bulky for EM, that is, with conventional EM methods.

At the molecular level, an outstanding achievement was to reveal the association of DNA with histones to form particles called nucleosomes. The DNA molecule, the double helix itself, is 2.2 nm in diameter and makes a full helical turn of 3.4 nm (along the spiral axis) for each length of 10 nucleotide pairs of the double helix (10.6 pairs for free DNA and 10.2 pairs for nucleosomal DNA).[12] Almost two (1.75) full rounds of DNA totaling 2×83 nucleotide pairs are wound round the periphery of the nucleosome, which is roughly a cylinder 11 nm in diameter and 5.6 nm thick. It contains an octomer histone core, 6.6 nm in diameter and 5.6 nm thick, composed of two copies of each of the four histones H2A, H2B, H3 and H4. From the nucleosomes, now studied in crystallography down to a resolution of 2.8 Å,[12] polypeptide chains of the histones stick out. This is considered to play an important part in the regulation of the DNA–histone core assemblies (assembly vs disassembly), chiefly by acetylation and deacetylation of the histone tails. The DNA and histone cores are linked into a polynucleosome: an 11-nm thick 'beads-on-a-string' fiber. 'Linker DNA' of various length, from 0 to 80 nucleotide pairs, connects the nucleosomes. In this 'beads-on-a-string' association the DNA is packed lengthwise in a proportion of 6 : 1.

Chromatin, i.e. chromosome fibers, is biochemically a poorly defined entity varying with isolation sources and conditions and is composed of DNA with histones and chromosomal nonhistone proteins. The beaded-string organization is observed when chromatin is isolated and treated in buffers (pH 7.4) at low, i.e. hypotonic, salt concentration (10 mM), depleted of the divalent cations Mg^{2+} and Ca^{2+}.[13] The required deficiency of divalent cations in the isolation procedures indicates that the rather loose beaded-string configuration cannot persist under physiological conditions. However, it is not known whether living cells are capable of regulating the concentration of the divalent cations intranuclearly.

In the presence of divalent cations, 1–5 mM Mg^{2+} or/and Ca^{2+}, in neutral buffers, the isolated chromatin fibers observed have a diameter in the range 20–50 nm, depending on the isolation conditions.[13] The size is in better agreement with that of the chromatin and chromosome fibers observed in isolated whole mounts of, e.g. metaphase chromosomes.[13]

The prevalent concept of the folding of the DNA into the 30-nm chromatin fiber structure is likewise attributed only to histones. In this configuration the 11-nm polynucleosomal DNA fiber is anticipated to fold into a 30-nm solenoid with the incorporation of a molecule of histone H1 to each nucleosome. The binding site of H1 at the nucleosome has been defined but the arrangement of H1 in the 30-nm fiber organization is unclear. Recent data have positioned the globular domain of H1 close to the dyad axis, in a polar arrangement of H1 molecules along the nucleosome fiber that may influence gene regulation in addition to its structural role.[14]

The perplexity confronted in understanding the 30-nm chromatin or chromosome fiber structure is evident from various studies.[15] The observations have resulted in numerous models that can be roughly classified as (1) the original solenoid model, (2) some kind of a helical coil of the nucleosome fiber, (3) a beaded (superbead, supranucleosome, nucleomer) arrangement of the nucleosome subunits[16] and (4) a continuously variable zigzag nucleosomal ribbon.[4] The irregular zigzag nucleosomal ribbon has support from electron tomography studies,[4] cryo-electron tomography[17] and recently radiation experiments on chromatin in studies on living cells,[18] affirming linker lengths of 40 nucleotide pairs for an idealized zigzag model.

Estimating that 6–7 nucleosomes of the polynucleosomal string condense into one turn of a 30-nm thick chromatin fiber, the length of DNA is reduced in the proportion of 40 : 1. To obtain the 10^4 : 1 packing in metaphase chromosomes, further packing of 250 : 1 is required.

The prevalent opinion about packing the 30 nm chromosome fiber further into metaphase chromosomes holds that the fiber folds are packed into loops that are fixed to a chromosome scaffold structure composed of nonhistone proteins.[19] Topoisomerase II has been shown to be a main component of the scaffold proteins, making its contribution decisively important in sorting out tangling DNA strands after replication, in the condensing of chromatin loops and in the separation of the daughter chromosomes at mitosis. In addition, as mentioned above, certain new scaffold proteins have been shown to be involved in the condensation of chromosomes and in the separation of sister chromatids in mitosis.[20]

The chromosome scaffold was originally revealed in preparations of isolated metaphase chromosomes treated with high salt buffers (2 M NaCl solution) or dextran sulfate–heparin, to extract the histones and other soluble proteins. The extracted chromosomes were spread on a hypophase of a hypotonic solution. In these preparations clouds of looped dehistonized DNA could be observed surrounding a residual chromosome that principally persisted in the shape of the original metaphase chromosome. Only a residual chromosome scaffold remained after DNase digestion. With the same methods, an analogous nuclear matrix, nuclear skeleton

or cage of interphase nuclei was isolated, surrounded by clouds of looping dehistonized DNA, when digestion with nucleases was omitted.[19]

These observations suggested a looped folding of the chromatin fibers around nonhistone chromosomal scaffold proteins[19] as the principle of organizing the 30-nm chromatin fiber in chromosomes rather than a coiled-coil model. Consequently, the size, association and configuration of the regions [called scaffold-associated region (SAR) and matrix-associated region (MAR)] of looped DNA with the scaffolding proteins have been the object of various studies for the past decades, but contradictions and perplexities have hindered satisfactory concepts.[19] For example, only a slight change in the conditions for the isolation of an interphase nuclear matrix[19] resulted in a residual NE composed only of a nuclear pore complex (NPC) lamina fraction, depleted of an internal nuclear matrix. This may indicate the delicate and dynamic association of chromatin with the NE.[8,21]

It is important to recognize the apparently different organization units of the different levels of chromosome organization: (1) the polynucleosomal DNA fiber, (2) the 30-nm chromatin fiber and (3) looping of the chromatin fiber somehow around the chromosome scaffold, forming the metaphase chromosome. In interphase nuclei, chromatin is organized around analogous structures, variously termed the nuclear matrix, scaffold or skeleton, which seem to be dynamically integrated with the NPC lamina of the NE.[19,21,22]

Although the principal organization of the repeated building blocks at each organization level must be uniform, the variations and complexity in these repeats seem to increase from level to level. At the 'beads-on-a-string' level, the unit is the nucleosome with the linking DNA. For the 30-nm chromatin fiber the unit is 6–7 nucleosomes forming one turn, as assumed in the solenoid model, or their arrangement is more variable and flexible, namely an irregular nucleosomal ribbon according to the zigzag model or, as assumed in the supranucleosomal chromatin model, 7–42 nucleosomes are packed into various-sized 30–65-nm supranucleosomal units.[23] At the next higher organization level the units are the loops bound by the scaffolding structures. The loop with an associated scaffold element seems to be the elementary building block towards higher chromosome organization. Variations of the loop sizes and the clustering of the loops into, e.g. rosette-like configurations have been observed and suggested in different instances.[21,22]

How, then, do we understand the organization of the chromomeres,[13,21,22] as described in the classical studies with LM? Chromomeres are best observed in prophase chromosomes of meiosis and they must in some way be folded by the 30-nm chromatin-loop organization with scaffold proteins.

Also, the bands seen in the giant polytene chromosomes of salivary glands in, e.g. *Drosophila* must in some way fit in, i.e. be a natural consequence of the folding of the 30-nm chromatin fiber. As polytene chromosomes represent tight lateral alignments of bundles of interphase chromosomes (up to 1024 chromosomes in *Drosophila*), the bands distinguished are considered to be apposed chromomeres[13] of interphase chromosomes. Thus chromomeres seem to be organizational entities also in the interphase and not only consequences of early prophase chromosome condensation. This indicates that the folding of the 30-nm chromatin loops is actually preserved in interphase chromosomes, if we assume that polytene chromosomes are not distinctive exceptions. In addition, the size difference of the bands in polytene chromosomes must also be a natural consequence of an adequate chromosome model.[21,22]

Chromosome coiling, i.e. the coiling of the cromonemata[13] in classical descriptions from early LM studies,[24] is another example of large-scale structural chromosome features that must fit with any presumed looping of the 30-nm chromatin with scaffolding proteins, if the model concerned is to be acceptable. In animal cells, chromosome coiling is not usually distinguished after ordinary treatment, i.e. without specific procedures.[13] However, even without any specific treatments it is observed in plants with very large chromosomes (e.g. in *Tradescantia*), and also in living plant cells[24] and in unfixed animal cells processed for EM.[25]

Significantly, chromosome coiling also appears when ordinary chromosome preparations are squashed in 50%[13] or isolated with 60% acetic acid (AA),[22] indicating that chromosome preparations isolated with detergents under 'physiological' conditions or water spread[13] somehow lose or disassemble the coiling. We can also presume that the banding technique that is used today in karyotyping might have the structural background in the underlying chromosome coiling, as has been suggested.[26]

Immunological methods for staining topoisomerase II (a main scaffold protein) reveal a clearly spiralized internal core in chromosome preparations, similar to chromosome coiling.[27] Also, 3-D reconstructions by electron tomography of chromosomes, after histone extraction and DNA digestion, appear as a coiled residual chromosome structure, indicating that chromosome coiling is maintained by scaffold proteins.[28] Accordingly, in chromosome condensation, the coiling is somehow brought about in the folding of chromatin fibers by the scaffold proteins. It remains to be shown if scaffold proteins, when successfully isolated and dissolved, will self-assemble to coiled structures, especially when affiliated with DNA and histones.

Textbook diagrams and models for the higher order chromosome structure fail in giving substantial structural reasons for the several intermediate folding levels from the 30-nm chromatin fiber up to metaphase chromatids.[29] Recent discussions,[30,31] and earlier reviews of chromosome structure[22] have tried to fill this gap. Having their particular merits, most chromosome models do not meet the criteria for an adequate and unifying model – those of comprehensively accounting for different-sized chromomeres of interphase chromosomes (e.g. polytene) and meiotic prophase chromosomes, for chromosome coiling and for the origin of

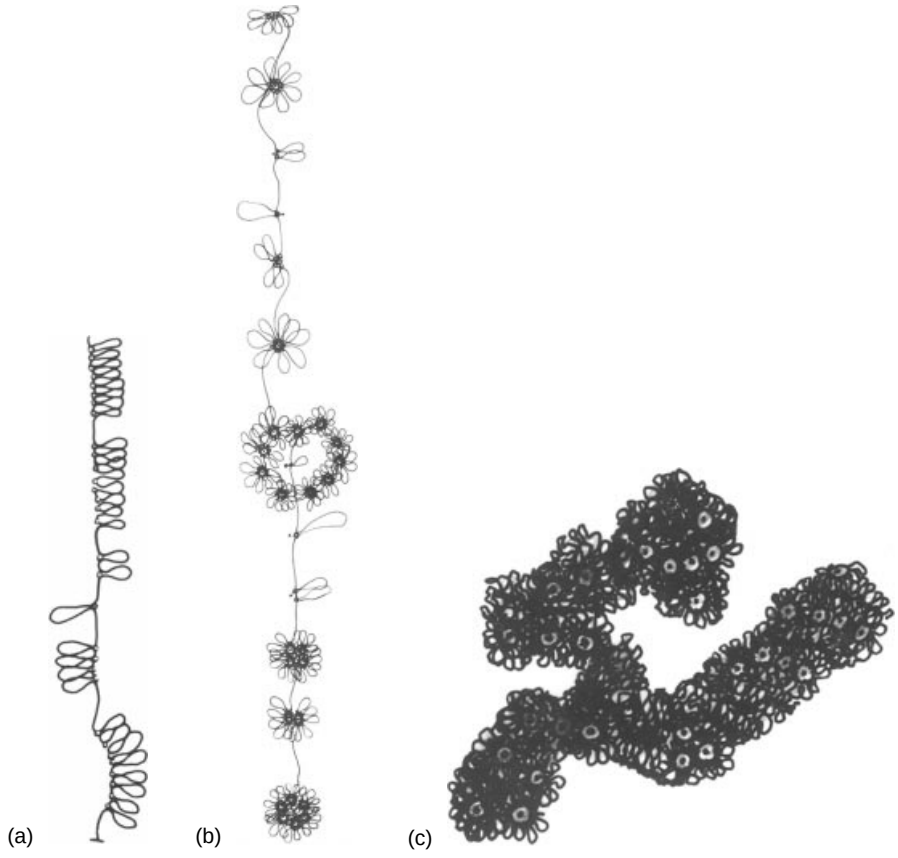

Figure 1 A unified model[8,21,22] of higher-order DNA (DNA loop or chromatin fiber) folding in chromosomes: the loop-and-rosette model. The different categories of data (e.g. polytene chromosomes, Figure 2) fit best with this model. From interphase to metaphase chromosomes. (a) Single (histone-depleted) DNA loops and accumulations (duplications) of these in linear form, i.e. total or strictly local unfolding of chromomeres in a chromatid. (b) Arrangement of various size classes and organization types of chromomeres in a partly stretched-out interphase chromatid. The folding of a continuous DNA by looping: single loops which would correspond to primary replicons; double loops, multiple loops and rosettes (around ring-like cores of scaffold elements, i.e. cyclomeres[8]) and their clustering; representing the origins for different-sized chromomeres during evolution. (c) The condensed form representing the metaphase chromosome. Ring-like structures are embedded in the chromatin. Note the similarity of appearance in a section of the premeiotic X chromosome of Acheta, (d), and in a stereo pair critical-point drying (CPD)-whole mount of a Chinese hamster ovary (CHO) metaphase chromosome (prepared as in section 2.4, Procedure: 1b) shown in (e). There is a complete analogy with a chromatid of the polytene chromosome. Only the condensation is different as no lateral apposition of chromatids occurs. Instead, a linear apposition causes chromatid coiling and linear condensation of the chromosome arms. This would be chiefly due, not to the condensation of interchromomeric DNA, but rather to the tendency of the chromomere core elements (scaffold elements, i.e. cyclomeres and their subunits) to interact and assemble. Proteins of these interactions have recently been identified as the SMC family among scaffold proteins.[10,20] This results in higher-order structures such as chromosome (chromatid) coils, in which chromomeres are arranged in analogy with nucleosomes in the models of 30 nm chromatin fiber, either as in the solenoid model[15] or as in the zigzag nucleosomal ribbon model.[4] (f) 3-D reconstruction of the chromosome shown in (e), from tilt series with 6° increments (section 4.2), with MEM (section 5.4), visualized with BOB (section 6.1), shown in stereo pairs (recorded with SNAPSHOT from Silicon Graphics Inc. (SGI) display). (g) Stereo views, with 10° increments, of the reconstructed chromosome in (f). Note that chromosome coiling is recognizable as chromosome banding and the impression of bands depends also on the viewing angle. (h) Stereo series as in (g). Details of the chromosome arms with coiling (arrowhead) and ring-like structures of cyclomere size (arrows), surrounded with looping fibers of hazy chromatin. Note that these fibers are not detected in the chromosome scaffold, Figure 8(a, e) (cf. the MEM/3-D reconstruction of chromosome scaffold Figure 8a, b, e). (Reproduced from Engelhardt.[22])

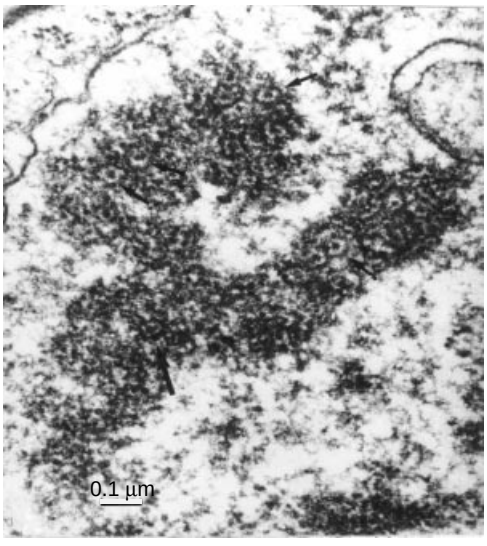

(d)

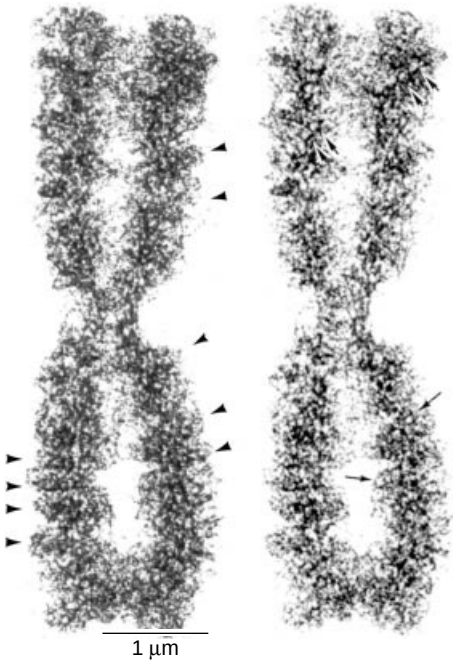

(e)

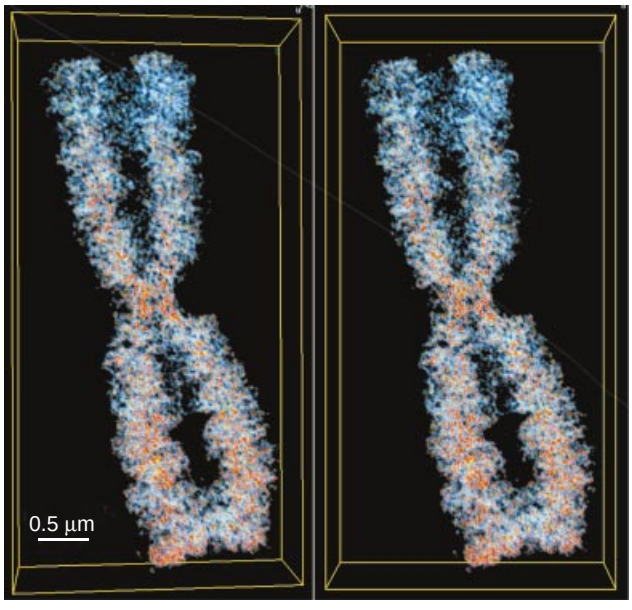

(f)

Figure 1 (*Continued*)

and interplay with the chromosome scaffold and nuclear matrix.

It is worth noting that, when the chromosome material (chromatin) coils and (therefore) compacts, the two levels of coiling, (1) the 11-nm fiber to the 30-nm fiber and (2) the extended chromonema to the compacted mitotic chromosome or chromatid, appear closely similar and suggest analogous configurations of condensation (solenoid and zigzag configuration, see the notes in the legend of chromosome model, Figure 1).

Our early investigation of chromosome structure,[8] with a unifying intent, started partly from theoretical postulates that motivated a search for adequate fixing and staining methods with ruthenium red (RR) (developed for intracellular staining, see section 3.5) for meiotic chromosomes in order to reveal details in the attachment of DNA to the NE and to the SC. The methods[8] revealed the distinct presence of ring-like cores (which we named cyclomeres) in the premeiotic X chromosome of *Acheta* and also along the lateral elements of the SC. The ring-like

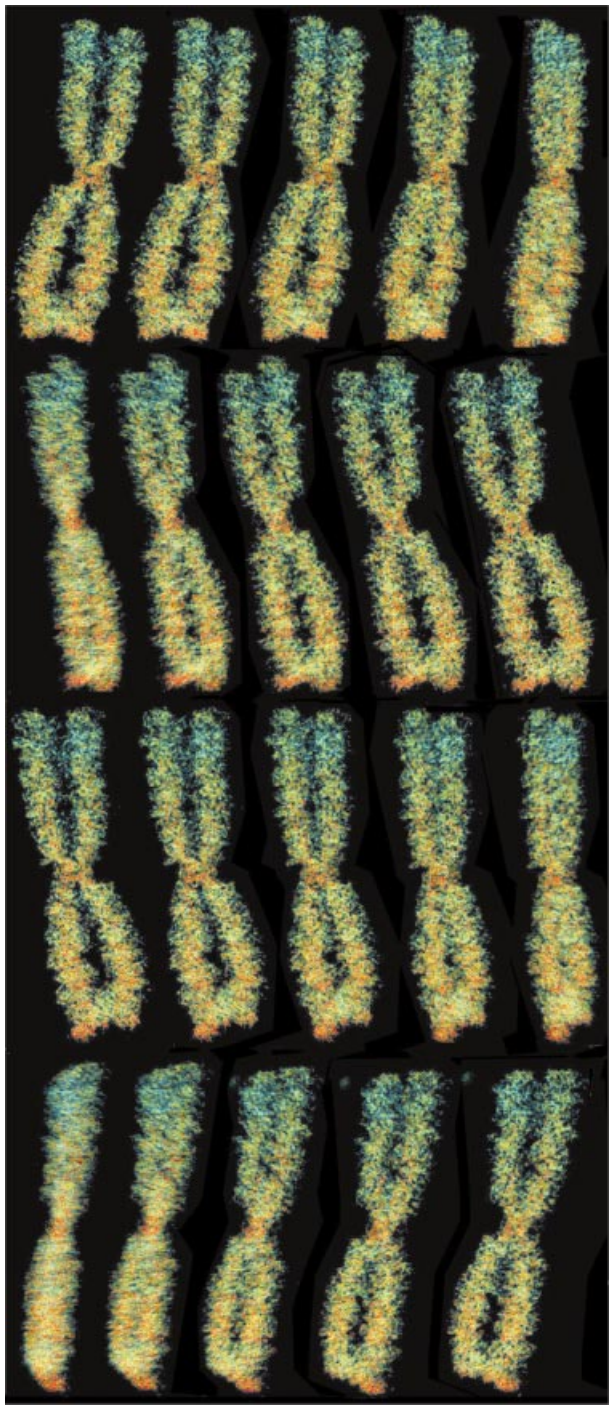

(g)

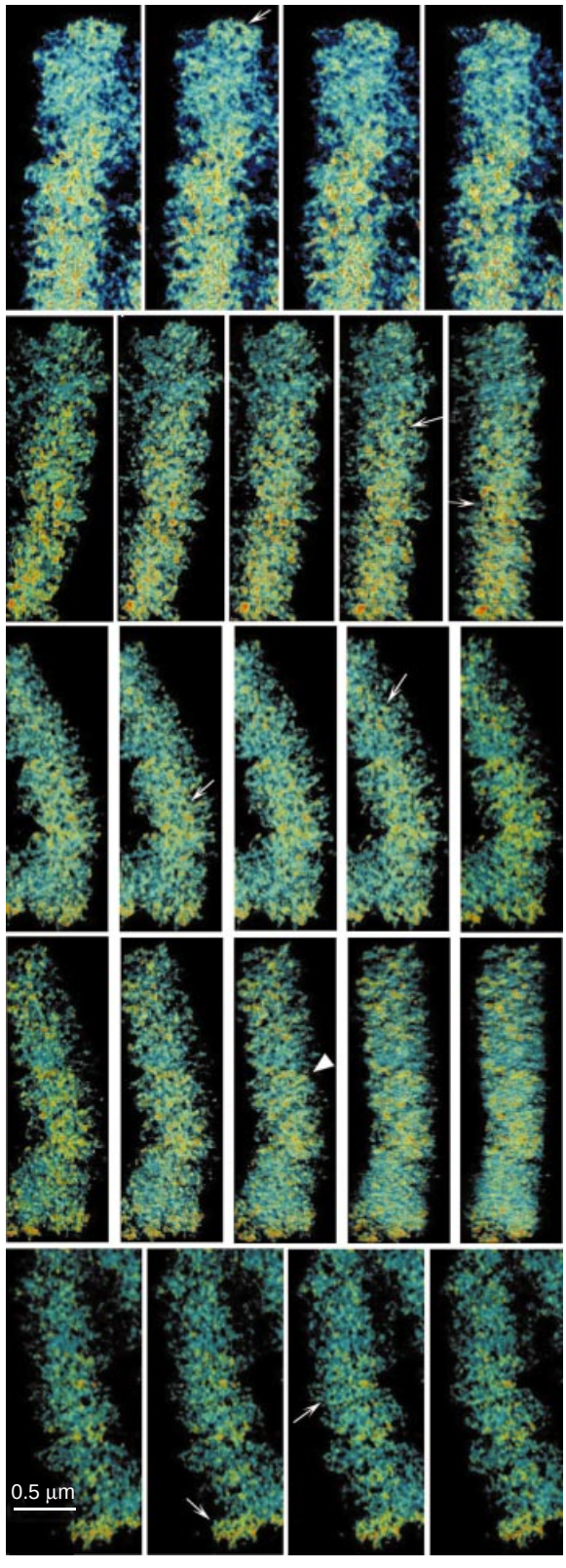

(h)

Figure 1 (*Continued*)

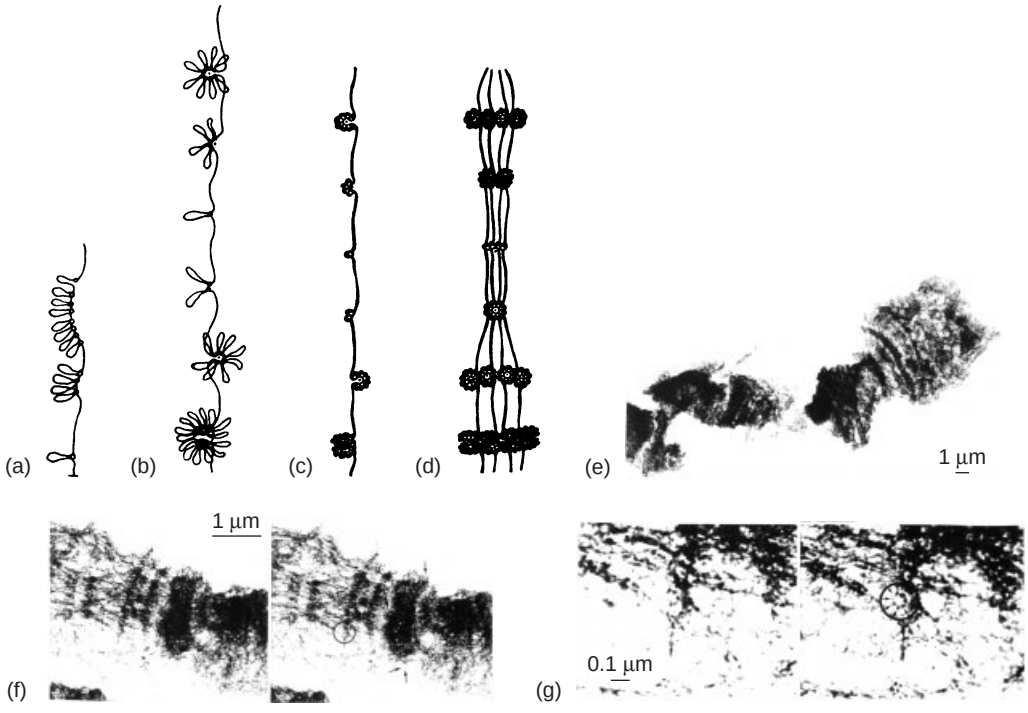

Figure 2 The loop-and-rosette model from interphase to polytene chromosomes. (a) As Figure 1. (b) As Figure 1. (c) As (b), showing that the small DNA loops (1.2–2.2 kb) as seen in polytene chromosomes,[21,22] are bound by 6–11 nucleosomes that form superbeads (30–60 nm in diameter, cf. metaphase chromosome, Figure 7), because of the short loop lengths associated with the scaffold elements. (d) Polytenisation: lateral apposition of chromatids (only four chromatids are drawn for clarity to show the principle), demonstrating the formation of the bands of different thickness. A constriction is interpreted as tendency for primary chromomeres (single loops) to fuse from separate chromatids, rather than as point of underreplication as has been formerly suggested (references in Engelhardt[22]). (e) General view of a whole mount of a CPD polytene chromosome (prepared as the metaphase chromosome in Figure 1e). (f) Stereo pairs of details at higher magnification. Ring-like structures (thin arrows) can be seen. In some rings (encircled) granular subunits are detected. (g) Ring-like alignments of scaffold-forming subunits (circles containing thin arrows) can be visualized in the bands, and they are similar to those found in metaphase chromosomes (cf. Figure 1e–h). This indicates that polytene chromosome bands are composed of the same scaffolding ring-like structures and subunits as metaphase chromosomes and this is best shown when the gross structure of the bands is also well preserved. (Reproduced from Engelhardt.[22])

structures could be traced to derivatives originating from the NE. More specifically, the structures appeared to be virtually identical with an apparently detachable nuclear part of the bipartite NPC. Striated microfilaments lining the lateral elements of the SC were revealed. Apparently, they connect neighboring cyclomeres and may represent the NE lamina. Certain lamina proteins have indeed recently been shown by immunoelectron microscopy (IEM) after DNase digestion to be present throughout the nuclear interior.[32]

It was suggested[8] that the DNA is folded around these ring-like cores, which function as the control elements for replication and transcription. The folding of DNA around these foci emerged as the most convenient way of packing DNA in interphase and metaphase chromosomes. The DNA folding (Figure 1) was presented as the loop-and-rosette model.[22] This implied a natural reason for the different sizes of chromomeres as arising naturally from replicon duplication and from the clustering of repeated replicons to rosettes. By the same principle, a model for polytene chromosomes was presented (Figure 2).[21,22] The details and consequences have been extensively discussed[22] in relation to the NE, chromosome scaffold and the nuclear matrix, and as resulting in the evolution of the chromosome structure.

This integrative model, in retrospect, involved details that strikingly resemble present-day concepts about the central control of replication machinery of eukaryotes. This machinery, with its rosette-like control elements, appears to be uniform from yeast to higher eukaryotes,[3,33] and the proposal of eukaryotic chromomeres as replication and transcription factories, also composed of rosette-form configurations, has been presented.[31] The protein composition of the replication foci involves different dynamically associated proteins, now identified.[33] A single (170-kDa) structural protein, called foci-forming activity (FFA-1), assembles as a ring-like core of the foci that generate the loop replicons. It is a novel protein according to limited sequence data.[33] It

remains to be seen if these proteins have any relationship with our early suggestions.[8]

1.2 Electron Tomography Compared with Earlier Methods

The theoretical resolution of TEM at 100 kV is 0.003 nm, which is sufficient for visualizing atoms (the van der Waals radius of the hydrogen atom being 0.12 nm and that of carbon 0.2 nm). In practice, owing to instrumental constraints and other restrictions that are difficult to overcome,[34] the resolution for modern TEM is at best 0.1 nm, which is still of the magnitude of atomic resolution accomplished, e.g. in TEM crystallography.[35] However, in biological samples the practical resolving power is often not better than about 1–2 nm. At least partly, this is in practice because details in images are in variable degrees superimposed owing to specimen thickness.

Inspection of stereo pairs greatly improves the actual resolution of structures under study, because it eliminates the superimposition of structures. This is accomplished with a mirror stereoscope (e.g. Old Delft, with auxiliary 4.5 × magnification) viewing photographic negatives in transmitted light. This technique has been found most useful and advantageous for interpreting bulky whole-mounted chromosome preparations after, e.g. digestion and treatment procedures.[22]

However, the modern 3-D approach is the ETM, i.e. TEM tomography,[36] to replace the static 3-D viewing of stereo pairs. TEM produces images that are orthogonal projections of the 3-D object under study. Tilt series of image projections of an object from 0 to $\pm 60^{\circ}$, with e.g. a 3° increment, are recovered with a eucentric goniometer specimen holder that is usually incorporated in a modern TEM instrument. The set of projections in tomography are named Radon transforms after Radon (1917), who first presented the mathematical (back-projection) method of rebuilding the original 3-D object from its projections.[36] It was only in 1968 that such an approach was put forward for 3-D reconstruction in TEM studies of biological samples,[37–39] authored in three independent papers.[40] At present ETM allows reproducible 3-D reconstructions with a resolution of 2.5–8.5 nm.[41]

Only in recent decades has ETM become a useful tool in structural biology[36,42] because of the great increase in computer power available. Chromosome studies have played a pivotal role in the development of ETM as described in a detailed review by Woodcock,[4] who also mentions that the MEM in ETM was first used in chromatin studies.[43] One of the first successful tomographic reconstructions of a whole-mounted chromosome (spread on water surface),[44] attempting to track[45] the folding of the chromatin fiber, was performed by a filtered back-projection method with an 'exact' filter algorithm.

The reasons why ETM has not yet become a widely used tool in structural biology were discussed at a recent meeting.[46] Earlier methods have been time-consuming in the extreme. It could take weeks or months to collect the amount of data that the present digital technology provides in days or hours. In addition, as the research community engaged in developing the methods has been rather small, the number of high-impact papers showing striking and convincing results is still relatively small. All this may soon change as programs, high-performance computing and instruments become available.

With the lack of efficient methods, biology has been working in a relatively flat world in trying to understand structures and functions at the molecular level. Yet these things occur in a dynamic 3-D environment. It is with ETM that we are beginning to have a closer look at this 3-D cell environment. In particular, there is at last a solid prospect of comprehending, with ETM combined with immunological,[47] in situ hybridization and with other methods, the higher order structure of chromosomes, the intricacies of which – as presented by the mingled 3-D hierarchy, the manifold of scaffold proteins,[10,11,19] and the DNA folding enigmatically connected with all this – have so far been next to impenetrable.

2 PREPARATION STEPS FOR CHROMOSOMES

2.1 General

As previously discussed,[4] there is in fact no consensus on how to prepare chromosomes for ETM investigation. In addition, ordinary EM fixation methods for, e.g. thin section studies are insufficient for revealing details in nuclear and chromosome configuration, as recognized earlier.[8] To show details of nuclei in sectioned material, staining and preservation with, e.g. various RR methods, as mentioned above, have proved to be more revealing.[8] Viruses with known surface decoration are useful as test objects for developing fixation and preservation methods for ETM.[28] Viruses can also be used as internal standards for evaluation of the 3-D preservation and resolution.

Most ordinary preparation methods used in TEM investigations are usually also convenient for ETM: (1) sections of epoxy resin embeddings, (2) whole mounts and (3) cryo-EM samples. All have their advantages and disadvantages. However, ETM has revealed shortcomings in some common preparative methods such as negative staining of, e.g. some viruses that appear very flattened (about 50%) in 3-D reconstructions.[28]

Reconstruction from sections of epoxy resin embeddings that are commonly used in EM may not be the best method. Sections, however, may often be the only choice to select an embedded specific object for reconstruction, e.g. chromosomes from certain tissue samples, cell aggregates or cultures. According to our experience, reconstructions obtained from sections are not usually as successful as those from whole mounts. The reason might be that sections suffer from various kinds of deformation that are not easily controlled, e.g. in cutting sections with the ultramicrotome and picking them on the grids, in addition to the observed thinning, up to 50%, of sections in EM, in the collection of tilt series.[4] Also, the signal-to-noise ratio is degraded in embeddings. Noise is a general problem also in cryo-TEM when unstained specimens are embedded in vitreous ice. However, the low signal-to-noise ratio may significantly be improved by removing the epoxy resin (or other embedding medium) from sections, thus making a kind of whole-mount preparation of these sections (section 3.5).

Whole mounts of, e.g. chromosomes are preferable for achieving a high signal-to-noise ratio and to secure that the whole content of the object under investigation is carried along. This is not always the situation for ultrathin sections. Sections of large organelles such as eukaryotic chromosomes and nuclei can, however, be of advantage when specimens such as whole mounts are too thick for ordinary 100–120-kV TEM; in earlier studies it was considered that 1 MV was the only choice for chromosomes,[13] for instance. Today, with modifications of preparative methods, 100–120-kV EM has proved sufficient for whole mounts, not only for whole-mounted chromosomes, but also various parts of whole-mounted cells.[47]

2.2 Chromosome Isolation and Whole Mounts

It is sufficient to present the main principles used in chromosome isolation methods because details of the various procedures developed over the years have been published and thoroughly reviewed earlier.[48,49] This equally applies to chromosome scaffold isolation,[19] where new chromosome isolation methods have been introduced.

If a high yield of chromosomes is required, chromosomes are isolated in bulk from synchronized cell cultures[49] of established cell lines that are used in cytological laboratories, e.g. HeLa (human) and CHO cells.

The procedure is as follows. Cell cultures in logarithmic growth phase, when the confluence of cells is 50–60%, are synchronized with the addition of (2 mM) thymidine in the cultivation medium and incubated for 16–22 h (depending on the cell cycle for cell lines used). The growth medium, with thymidine, is replaced with a fresh medium including a mitotic inhibitor, e.g. (0.06–0.1 $\mu g\,mL^{-1}$) Colcemid (nocodazole or vinblastine for certain cell lines), with more (10–20%) than ordinary (5%) calf serum, or fetal calf serum, and incubated for 8–12 h. Cells in mitosis are released, naturally or aided by gentle shaking, into the growth medium, because in the cell lines to be used (e.g. HeLa, CHO) mitotic cells are rounded up and detach from the bottle surface. Mitotic cells are collected from the medium by centrifugation.

It is generally essential for a successful isolation of metaphase chromosomes with most of the chromosome isolation methods used that mitotic cells are swollen by hypotony by dispersing the pellet of mitotic cells in a hypotonic solution, e.g. 75 mM KCl, for about 10 min, at room temperature (RT) or at 37 °C. Some cells need first to be washed with the hypotony solution to make the hypotony treatment effective. The swollen cells are then collected gently by centrifugation, e.g. at 800–1000 rpm for 5–10 min. The total treatment time, including the centrifugation, must not exceed 15 min. This is important when divalent cations (Mg^{2+} and Ca^{2+} or polyamines), that are essential for chromosome stabilization, are not present (but see Mendelsohn,[49] with divalent cations present).

After the hypotony treatment, any of the various chromosome isolation procedures,[19,48,49] 'physiological' or less physiological, are convenient.

The only general requirement for isolating chromosomes and nuclei and keeping them stable, with e.g. 5–10 mM (or lower) *N*-(2-hydroxyethyl)piperazine-*N*′-(2-ethanesulfonic acid) (HEPES) buffer at pH 7.4, appears to be the presence of divalent cations (1–5 mM Ca^{2+} and/or Mg^{2+}) or polycations such as spermine (0.0125 mM) and spermidine (0.05 mM).[27] Monovalent salts only tend to cause aggregation.

Mitotic cells are also suited for the microspreading methods of mitotic[50] or meiotic chromosomes,[51] either without or with hypotony treatment.

The procedure is briefly as follows. In this method the cells are spread on water, or on hypotonic salt solution for more gentle spreading (0.05–0.1 M NaCl), to control better the spreading forces at the hypophase that break the cells and release the chromosomes. The chromosomes are picked from the hypophase surface on poly-L-lysine (PL) (below) or glow-discharged[51] carbon–Formvar-coated grids, after dehydration in methanol (MeOH), lightly stained with (0.001–0.002%) uranyl acetate (UA) in MeOH (30 s), washed in MeOH and dried by CPD (section 3.1).

With this elegant method, the chromosome preparations are ready for EM, without laborious purification and isolation procedures. There is the disadvantage that cytoplasmic obscuring components may also attach on the grid preparations. It is for the investigator to choose

the chromosomes on the grids, which does not seem to be too difficult a procedure as we can see in, e.g. DuPraw's splendid pictures of spread chromosomes.[5]

From the viewpoint of early chromosome morphology, these isolation methods yield the unexpected result that chromosome coiling is indistinct after any of the 'physiological' isolation or spreading methods, especially at neutral pH. The reason for this is not clearly understood.[13] Chromosomes squashed in 50% AA[13] after standard cytological fixation in MeOH–AA (3:1) do show distinct coiling.

Chromosomes isolated in bulk in 60% AA, after hypotony treatment, surprisingly show the same chromosome coiling[22] when the loose pellet of swollen cells is washed and dispersed in 60% AA. This method works also for cells that have been fixed, and stored at −20 °C, in MeOH–AA (3:1). The pellet of chromosomes, after centrifugation (1500–5000 rpm, 10–15 min), may appear indistinct depending on the initial amount of cells used. In any case, the pellet is washed in 60% AA, two or more times, and collected by centrifugation. After washing in 60% AA the chromosomes are diluted in a small amount of 60% AA and stored at +4 or −20 °C. After this procedure, a suspension of pure chromosomes, with 10–30% prophase and interphase nuclei, is found, with insignificant amount of cytoplasmic debris, when investigated by phase-contrast microscopy. Distinct chromosome coiling is visible with phase-contrast microscopy. The chromosomes do not aggregate when pelleted by centrifugation and the pellet is easily redispersed.

Polytene chromosomes can also be isolated by this method but to release them from nuclei they have to be spread on, e.g. 60% AA.[22] The chromosomes are then picked on polystyrene-coated grids (below), dehydrated, lightly stained with UA (above) and CPD (section 3.1) or *tert*-butanol dried (section 3.2).

In the AA-isolated metaphase chromosomes, the clearly preserved coiling matches classical chromosome descriptions. Thus, the AA-isolated chromosomes seem to be tempting objects to use to study the higher order chromosome structure related to chromosome coiling.

The metaphase chromosomes are mounted on EM grids by centrifugation (1–5 min, 500–1500 *g*) of a sample (5–10 µl of diluted chromosome solution, or 2–3 µl of the loose pellet) through a cushion of 60% AA, in microchambers (Figure 3) for grids (50–200 µl).

The centrifugation for mounting chromosomes on the grid is preferred as chromosomes are better preserved in their 3-D configuration than with other more direct application methods.

With AA, Formvar or carbon–Formvar-coated grids are not suitable, as they are not resistant to AA. However, grids coated with plastic (polystyrene) films (Petri dish pieces, e.g. Nunc, Nalge Nunc Inc., dissolved to make a 0.5% solution in 1,2-dichloroethane), without or with additional carbon coating, are resistant to AA.[22] These films are stronger than Formvar films but less adhesive. To prevent the film peeling off the grids, the latter may first be treated with an adhesive solution (0.01% polystyrene in benzene).[51]

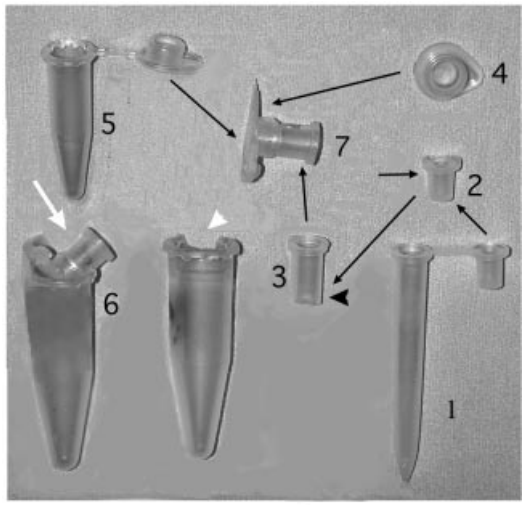

Figure 3 Grid microchambers are made of plastic hematocrit tubes (1). The plug (2) of the tube is cut off (arrow) so that the plug can be easily forced to the required depth (arrowhead), into the cut-off top part (3) of the hematocrit tube to function as the bottom for the grid. Chambers of suitable sizes are thus easily obtained, e.g. 50–200 µL. The caps of a 0.5 mL microcentrifuge (Eppendorf) tubes (4) are used as adapters for (3) fitted to 0.5 mL micro-centrifuge (Eppendorf) tubes (5) (which fit into to a larger tube for a swing-out desktop centrifuge, not shown). When a swing-out desktop centrifuge is not available, the 0.5 mL cap is positioned in a 45° angle (white arrow) in a 1.5 mL microcentrifuge (Eppendorf) tube (6) with a u-form cut (white arrowhead) for the grid microchambers (7), as a substitute in a swing-out position to have the sample evenly distributed over the grid. If high centrifugation speeds (over 1500 rpm) are used, the caps at 45° angle must be fixed (glued or melted) to be kept in place. These chambers are analogous to Miller's grid chambers,[53] but faster and easier to make.

Before mounting chromosomes on the grids, fiducial gold markers that are needed for the alignment of the images of the tilt series for ETM are applied on the grids. Ni or Au grids are preferable as in the presence of gold Cu will wither when stored. Colloidal gold markers are applied by dipping the grid, one or both sides, in a drop of, e.g. 5-, 10-, 15- or 40-nm colloidal gold solution diluted to, e.g. 1:10, with filtered double-distilled water ($FddH_2O$) (0.22 µm filter, Millipore) or with PL, e.g. 0.01–0.1 mg mL^{-1} in $FddH_2O$. Being uniformly more round and less liable to aggregate, commercial immunogold particles (e.g. expired) are more advisable than self-made particles. The grid, with adhering gold suspension, is immersed in 100% MeOH that precipitates the gold on the grid. This procedure is repeated, if

necessary, to obtain the amount of gold needed. The minimum number of gold markers is three [or four[52]], preferably 8–12 or more, for the image area and the magnification used. The same gold particles must be identified on each image in a tilt series (from 0 to ±60°, e.g. in 3° increments). The size of gold particles chosen depends on the magnification that will be used for the reconstruction. In addition, a mixture of different-sized gold particles is useful for different magnifications. With PL, the dilution of the gold suspension may be increased to a much higher degree. However, we observed the drawback that when embedded in PL the gold markers look less sharp and are difficult to distinguish, especially at high tilts.

2.3 Pretreatments: Salt Extraction and Enzyme Digestions

When the chromosomes are mounted on grids, they are ready for further procedures for EM. If salt treatments or enzyme digestions are required, they must be completed at this stage, before postfixation and staining are performed.

Note that the methods that follow are suited also for other than AA-employing chromosome isolation methods[48,49] and for microspreading methods.[50,51] The point is that the chromosomes are attached on grids for easy transfer to different solutions used.

The attachment of isolated chromosomes with centrifugation, in the isolation buffer used, is secured by treating the carbon- and film-coated grids with, e.g. PL (0.1–1 mg mL^{-1} in FddH_2O), for about 1–5 min, followed by washing in drops of FddH_2O. Also, glow discharging makes the carbon or plastic film coating hydrophilic and contributes to attaching chromosomes on the grid surface.[51] The same effect is obtained by UV radiation (10–30 min) or dipping in alcohol followed by air drying (AD).

These procedures are not necessary with AA-isolated chromosomes, as they do stick on hydrophobic polystyrene film-coated grids with carbon or not. Also, PL does not harm the attachment of AA isolated chromosomes.

To remove the grid easily from the microchambers after centrifugation, follow a simple procedure.[53] After centrifugation, add 60% AA to form a convex surface in the micro-chamber. Retrieve with curved anticapillary (and antimagnetic, for Ni grids) forceps by flipping the chamber upside down to let the grid float on the surface of the hanging drop. If the grid does not detach from the bottom by slightly rocking the microchamber, it can be released by touching with a thin needle or one arm of the thin forceps on the periphery of the grid.

Grid washings, etc. are accomplished in, e.g. a large Petri dish, with moistened filter-paper, overlaid with Parafilm. The Parafilm is preferably provided with drop-sized depressions (Figure 4).

The grids are washed in HM (10 mM HEPES, pH 7.4, 5 mM $MgCl_2$) or HC (10 mM HEPES, pH 7.4, 5 mM $CaCl_2$) buffer on the Parafilm, with several droplets (1–5 min in each) to remove the AA and to balance the pH to neutral. AA-isolated chromosomes retain their morphology when transferred to water solutions containing divalent cations at neutral pH. (For a routine, it is recommended to use double-distilled water, and filter (0.22 μm, e.g. Millipore) all solutions. Also use rubber gloves, wash if powdered.)

To isolate the chromosome scaffold, histones are extracted with, e.g. 2 M NaCl solution and digested with DNase and RNase.[21,22]

However, chromosomes isolated with 60% AA, according to our sodium dodecyl sulfate polyacrylamide gel electrophoresis (SDS/PAGE) analysis and immunoblotting, show no or negligible amounts of histones,[54] the bulk of which appears in the primary 60% AA extract.

Thus extraction with 2 M NaCl-solution apparently is not necessary to extract histones. In any case, digestion with DNase I (10 μg mL^{-1}) (Boehringer), with or without RNase A (10 μg) (Boehringer), completed in 2 M NaCl in HM buffer, shows better results when monitored with DNA-specific fluorochromes, e.g. DAPI (4′,6-diamidino-2-phenylindole) (Sigma), 0.25–0.5 μg mL^{-1}, in the digestion solution.[22,54]

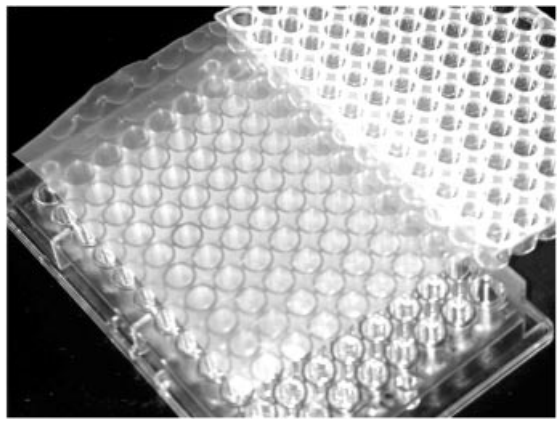

Figure 4 Depressions on Parafilm are obtained as follows. Take two incubation chambers with 96 wells, one with round-bottomed wells, frames removed. After inserting Parafilm (with its cover paper, not shown) between the two chambers, press together. The 'dimples' formed will ensure that the incubation drops (about 50 μL) do not float around during washing steps, when positioned in a large petri dish with moistened filter paper (to prevent the drops from drying during incubation).

After DNase I digestion in 2 M salt–HM buffer for 1–2 h at RT, no DNA-specific fluorescence can be detected after washings in 2 M salt–HM buffer followed by washings in HM buffer, and mounted in DAPI mounting medium (MM) (90% glycerine, 0.25–0.5 $\mu g\,mL^{-1}$ DAPI, in HM or HC, with antifading substances such as 10–20 mM dithiothreitol or 2-mercaptoethanol). Many commercial antifade/bleaching embedding products are available (note that the presence of divalent cations is necessary for the stability of isolated chromosomes).

Any other enzyme digestions desired are performed similarly [cf. hyaluronidase[21,22]], sequentially or if possible simultaneously, in the buffer solutions required.

Control preparations are made in the same salt buffers but without the enzyme, denatured enzymes or with enzyme inhibitors.

For enzyme digestion of resinless thick sections of whole-mounted cells, see section 3.5.

2.4 Fixation of Chromosomes

Chromosome preparations, with or without various pretreatments, preferably are chemically postfixed with glutaraldehyde (GA), a cross-linking substance and a reliable preserver of cellular ultrastructural details. Our purpose is to maintain the chromosome coiling for 3-D reconstruction. AA is not a cross-linking fixative but preserves the higher order chromosome structure, e.g. chromosome coiling, by acting as a precipitator of chromosomal nonhistone proteins. As mentioned, there is no consensus on how to preserve chromosomes for ETM,[4] so the field is open to the development of new fixation methods for testing and refining. Cautious fixation and staining are important especially after digestion–extraction steps when the residual delicate material left might easily be lost in washing steps or the configuration might change during dehydration steps before, e.g. CPD (section 3).

We have found it advantageous to use a set of various fixation procedures as a standard protocol to test different constituents and their combinations on the 3-D structural preservation and appearance. This concerns not only methods for structural chromosome studies but also any other material such as whole-mounted cells, e.g. in developing IET[47] methods (section 7).

Fixing and preserving whole mounts is a delicate procedure, as too much contrast, i.e. electron density, must be avoided to keep specimens transparent, when conventional 100–120-kV TEM is used for collecting the tilt series. The methods used in standard thin-sectioning studies, where high contrast is rarely a problem, will not work well if not modified. Little attention has been paid to developing preparative methods for whole mounts for TEM. The quality of ETM 3-D reconstructions depends as much on the development of programming methods and the performance of TEM as on the development of specimen preparative techniques suited for ETM, just as early EM depended on the instrument but equally on developing specimen preparative techniques.

CPD and other 3-D preserving methods (section 3) are used to avoid drying artifacts after the fixation procedures. It has been reported,[55] however, in scanning electron microscopy studies, that GA shrinks cells to some 45%, despite CPD. The shrinking by GA was prevented by using tannic acid (TA), after osmium tetraoxide (OT) fixation.

We tested the TA procedure using viruses as test objects. We had previously found that viruses fixed with GA appeared slightly smaller than recorded in the literature, after drying from solidified *tert*-butanol (analogous to CPD, section 3.2) for 3-D reconstructions by ETM.[28] With TA included in the fixation procedures, the size of the viruses appeared more in accordance with the reported sizes of the viruses (unpublished work).

Upon testing the TA method on chromosomes, the chromosome fibers appeared significantly thicker (40–60 nm) than chromatin fibers without TA (35–40 nm). In addition, the chromosome fibers appeared to be composed of supranucleosome-like particles of various sizes rather than a more regular fiber that the solenoid model predicts (cf. Figures 5 and 6 with Figure 7). In addition, the organization of the chromosome scaffold fibers changed appearance with TA.[54]

In our present standard fixation protocol, TA is included with GA, OT and UA with some modification of the original method.[55] Fixation controls, to test the effect of the different substances and their combinations, are used.

Dehydration and staining with UA (0.001–0.002%) in MeOH are performed in microcentrifuge tubes (Eppendorf) (1.5-mL test tubes). Curved anticapillary (and antimagnetic, for Ni grids) forceps are advantageous in the transferring steps.

The procedures are as follows. The fixation and preserving methods, for AA-isolated chromosomes and chromosome scaffolds, are accomplished with chromosomes mounted on grids:

1. (a) No postfixation;
   (b) boiling in 50% AA, for 30–60 s,[21]
   (c) wash, 3–5×, in HM or HC buffer, if the specimens are brought to salt and enzyme treatments, section 2.3;
   (d) dehydration (30, 50, 75, 100%, 10–30 s per step) in MeOH;

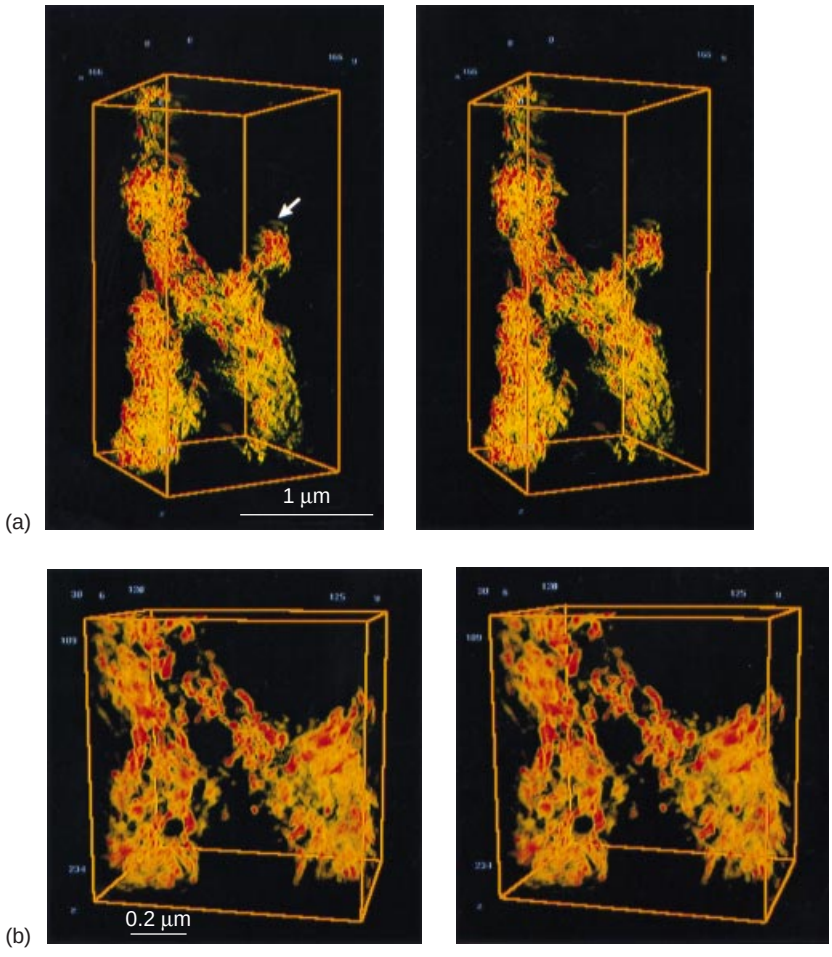

Figure 5 (a) Example of a low-resolution 3-D reconstruction with weighted back-projection method (WBM) of AA-isolated (HeLa) metaphase chromosome (prepared as in section 2.4, Procedure 1(b), and dried from *tert*-butanol, section 3.2), visualized with BOB (section 6.1; Figure 1f). The WBM has been low-pass filtered to 25 nm. Chromosome fibers of 25–60 nm are seen. Streaks seen in depth direction are artifacts that appear with WBM due to the missing data and other discrepancies (e.g. alignment inexactness, when tilting parameters are not accurately determined, especially with the angle of tilt axis being manually approximated, produces whirl-like streaks, arrow, in the reconstruction). [Reproduced by permission of the Center of Scientific Computing from Engelhardt et al.[28] and also from Engelhardt and Ruokolainen.[54]] This case of ETM, scanning, alignment and WBM was processed with the programs developed in Dr U. Skoglund's laboratory, Department of Cell and Molecular Biology, Karolinska Institute, Stockholm, Sweden, in 1993. (b) Details, in stereo pair of (a), at higher magnification. Chromosome fibers (20–60 nm) appear smoothed (low-pass filtered) with no sub-details detectable.

(e) staining in (0.001–0.002%) UA in MeOH for 30 s, wash in MeOH (3×);

(f) drying, with 3-D preservation methods, e.g. CPD (section 3);

Comment: boiling in 50% AA[22] causes additional purification of chromosomes from histones and cytoplasmic fragments.

2. Rapid TA method for chromosomes, modified from:[55]

- washing in HM buffer (3–5×);
- fixing, for 2–5 min, in mixture (1 : 1) of:
  1% GA in HM buffer, pH 7.4;
  0.5% OT in 0.1 M sodium cacodylate (NC) buffer, pH 7.4;
- washing in HM buffer (3–5×, 0.5–5 min);
- 0.5% TA in 0.1 M NC/HM buffer (1 : 1), 5 min;
- washing in HM buffer (3–5×, 0.5–5 min);

(a) staining with (0.001–0.01%) UA in FddH_2O, 5–10 min;

(b) without UA in FddH_2O:

- dehydration, staining in UA in MeOH, and drying as in (a).

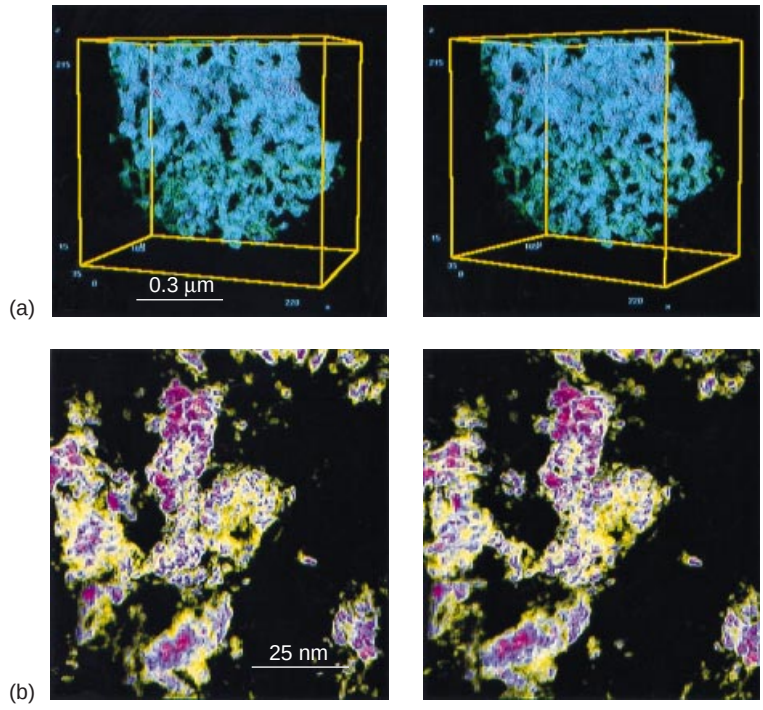

Figure 6 (a) Chromosome (HeLa), prepared as in Figure 5, showing 3-D reconstruction with MEM (section 5.4) of a chromosome telomere, in stereo (see above). (The original magnification of the tilt series was 48 000×, scanning pixel size 20 µm, giving the original resolution as 0.42 nm. With 6 × binning, the voxel size is 2.5 nm for the volume, i.e. the 'conservative estimate'[52] of resolution is not better than about (2–4) × 2.5 nm = 5–10 nm.) Some details (cf. Figure 5a) of chromosome fibers may be detected even at this low magnification. (b) At high resolution, the chromosome fibers appear decorated with details, but are difficult to interpret. Histones are extracted by AA but DNA is present (cf. immunoblotting analysis of histones and DNA fluorescence with DAPI in Figure 8d). [Reproduced from Engelhardt and Ruokolainen.[54]]

Controls and modifications:

3. as in 2, but without TA;
4. as in 2, but without OT;
5. as in 4, but without TA;
6. as in 3, but without UA.

3 PRESERVATION METHODS FOR THREE-DIMENSIONAL RECONSTRUCTIONS

3.1 Critical-point Drying

After fixation, the whole-mounted preparations have to be dried. AD causes artifacts, shrinkage, wrinkling and distortion that destroy the 3-D configuration. Drying artifacts are caused by disruptive effects of the surface tension of the fluid from which they are dried, e.g. water but also substances such as alcohol, used for dehydration, have a surface tension high enough to destroy delicate 3-D configurations.

The problem was recognized and solved in the early development (1950) of TEM techniques by T.F. Anderson, who introduced the CPD method.[50] CPD is conventionally used for whole-mount studies with scanning electron microscopy. CPD needs, however, an apparatus where the procedures are performed at high pressure.

CPD can be briefly described as follows.[50] After the grid samples have been gradually dehydrated in steps, e.g. in MeOH, the grids are put in a grid holder in the CPD apparatus, with some dehydration fluid, and the MeOH is completely replaced with liquid carbon dioxide (CO_2), at a high pressure (60–65 atm) in several (7–10) washing steps with liquid CO_2. CPD is completed, at an elevated pressure of about 100 atm ($P_c = 73.8$ bar), by increasing the temperature to ca. 40 °C. Keeping the temperature above the critical point temperature ($T_c = 31$ °C), the pressure is slowly decreased, regulated by a relief valve. After CPD, the specimens are ready for TEM.

However, CPD has some disadvantages such as causing thermal and pressure stresses in the specimens that may be difficult to avoid. An apparatus is needed for the procedure that may not always be available. The procedure needs liquid CO_2, preferably dried to remove

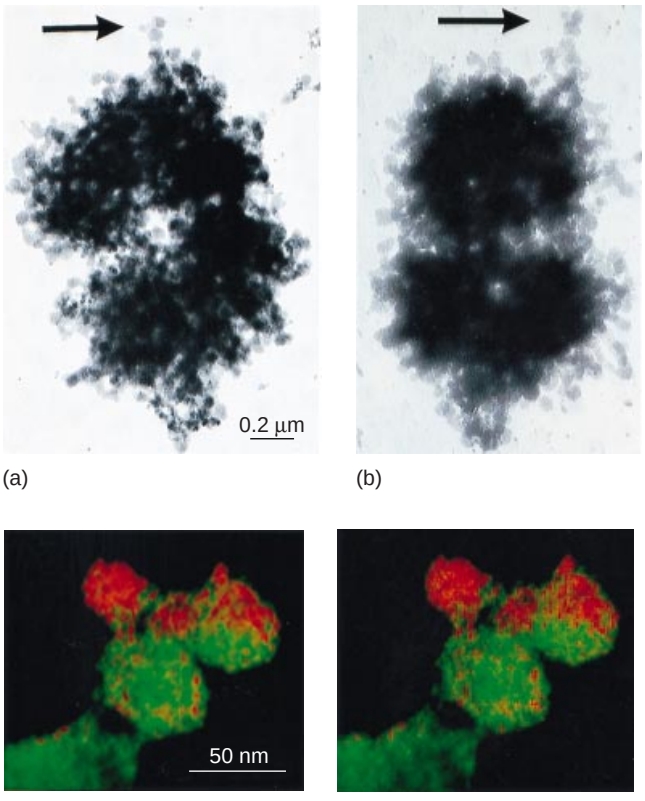

Figure 7 Chromosome (AA-isolated from HeLa cells), pretreated with TA before CPD to avoid shrinkage (section 2.4, procedure 2): (a) original tilt series at 0° tilt [reproduced from Engelhardt and Ruokolainen[54]] and (b) +60° tilt with mean diameter of the 30 nm chromatin fibers (arrow) increased to 30–60 nm with globular domains 30–60 nm in diameter. (c) Stereo pair of 3-D reconstruction with MEM (section 5.4) of the chromosome fiber [shown in (a) and (b) with an arrow]. The 30–60 globular domains of the chromosome fibers appear decorated and seem to be connected by two (2–4-nm) thin strands. [Reproduced from Engelhardt and Ruokolainen.[54]]

minute amounts of water that may be present.[56] The water present in liquid CO_2 was shown[56] to be the reason for drying artifacts such as thickening of cytoskeleton fibers in the microtrabecular lattice.[57] In addition, the CPD procedure takes time to finish.

3.2 Drying from *tert*-Butanol

When an apparatus for CPD is not available, a substitute for CPD is drying of the grid samples infused with *tert*-butanol. This method needs no expensive accessory, although such an apparatus has been constructed.[58] The procedure is much faster than CPD and is claimed to give analogous results. The method is easy to accomplish, with only a few restrictions, as ordinary grids coated with Formvar are not resistant to *tert*-butanol. However, plastic films (section 2.2) that are resistant to 60% AA used in chromosome isolation with an AA procedure are suitable for *tert*-butanol drying. In addition, grids with a pure carbon film coating are usable.

After the dehydration steps with, e.g. MeOH (and staining with UA in MeOH) of the grid samples, microcentrifuge tubes (Eppendorf) (1.5 mL) are used: one tube with a mixture of MeOH–*tert*-butanol (1 : 1), and then a series of 3–4 tubes with 100% *tert*-butanol (*tert*-butanol is liquid at temperatures above 25.5 °C). The grids are washed in each step for 10–60 s. After the last step each grid is dropped to the bottom in a separate microcentrifuge tube (Eppendorf) (1.5 mL) with about 0.5 mL of *tert*-butanol until all grids are ready. After infiltration with *tert*-butanol, the fluid is changed several times, if considered necessary, by gently pouring off the liquid, keeping the grid on the bottom. For the drying procedure a small amount of *tert*-butanol is left, letting the grid attach by capillary force to the wall of the tube, then sucking the fluid droplets left on the bottom with a pipet before closing the tube. The preparations are left for a short time in a cold place (below 25.5 °C), or briefly on ice, to let the *tert*-butanol solidify. The sample-containing tubes, with lid open, are brought to a vacuum drier (e.g. Savant Speed Vac Concentrator, with centrifugation off) to let the *tert*-butanol dry off. The grids are usually seen to drop to the bottom of the tubes when the drying is completed. The operation will not take longer than 10–30 min, depending on the amount of *tert*-butanol and the degree of vacuum used. The grids must be at RT when the preparations are lifted out from the vacuum dryer, to avoid water condensing on the specimens.

3.3 Freeze-drying

Freeze-drying (FD), like CPD, needs expensive equipment. The advantage of FD over CPD and drying from solidified *tert*-butanol is that the preparations are not dehydrated with organic substances that might be destructive, extracting membranes and denaturing proteins. Partial FD is used in the freeze-etching method, where cell preparations are coated with Pt–carbon to obtain replicas of, e.g. the cell cytoskeleton, showing sharp views of actin bundles and tubulin fibers in stereo.[59] However, replicas are not useful for ETM 3-D reconstructions as the entire preparation must be transparent and not only a surface view. When FD is adapted for ETM, the time must be extended (1–3 h) so that the drying of the specimen is completed. The specimens must be prewashed with FddH_2O to remove salts that will otherwise crystallize. If samples cannot maintain their configuration without salt, a volatile salt, e.g. ammonium acetate, is used at a concentration that keeps the specimen stable. Negative staining methods, e.g. of viruses, combined with FD

look superior[60] for 3-D reconstructions, as the specimen configuration is maintained and not flattened as with AD.

In brief, the procedure to freeze the specimen for FD is analogous to cryo-TEM methods. The specimen is frozen in liquid nitrogen, with a container with cryogen (e.g. liquid ethane or propane), as an intermediate fluid that is functioning as an effective conductor, for rapid freezing of the water-embedded specimen into vitrified ice. The FD is performed by raising the temperature (to −80 °C). Drying out of the preparation at high vacuum will then be possible within a reasonable time,[60] after which the preparations are ready for ETM.

3.4 Cryo-electron Tomography

Automation programs for collecting tilt series in ETM have made it possible, for 3-D reconstructions, to use single-axis cryo-ETM to collect tilt series of frozen vitrified samples, i.e. fully hydrated specimens, which are chemically unfixed, i.e. close to native state.[40] However, with this almost ideal method for specimen preservation a computer-controlled TEM and goniometer stage with cryo-holders, cooled with liquid nitrogen and accessories for preparing vitrified cryo-samples, are needed. A disadvantage is that the signal-to-noise ratio of the images usually tends to be poor, especially of unfixed and unstained specimens embedded in the vitrified ice. The noise in images is also difficult to abolish for specimens such as chromosomes as images collected in tilt series with axial tomography cannot be improved by any averaging image processing, as is possible with single particle or icosahedral virus tomography.[36,42]

The procedure is as follows. Use isolated chromosomes mounted (section 2.2) on grids, coated with perforated carbon, or better with perforated plastic film,[61] on, e.g. 50–75-mesh Ni or Au grids with colloidal (e.g. 5, 10, or 15 nm) gold markers for collecting tilt series. The idea with perforated-film coatings is to collect images of chromosomes that are preferably spanning a hole, embedded only in vitrified ice without a support, thus reducing noise and improving image contrast. Using 50-, 75-mesh or even single-slot grids, the prospect of viewing the whole tilting range from $0 \pm 60^{\circ}$ is considerably improved. The grid–specimen is washed in HM or HC buffer (≤5 mM HEPES buffer), in several droplets, before the grid, after excess buffer has been blotted off with filter-paper, is quickly dropped in a container, inserted in liquid nitrogen containing liquid ethane or propane, or better, in a mixture of ethane and propane (3 : 1) that prevents solidification of the freeze-transferring cryogens. The grids can be stored in liquid nitrogen until examination. The grid–specimen is installed in a liquid nitrogen-cooled cryo-specimen holder that protects the specimen from atmospheric humidity before cryo-TEM.

With cryo samples, automatic collection of the tilt series is the only way to avoid melting and beam damage of the specimens, as automation will shorten the exposure 10–100-fold compared with manual methods.[40]

3.5 Section Preparations

Our 3-D reconstructions with ETM, accomplished on sections of epoxy-embedded material, are not so successful as with whole mounts. Many reasons may account for this difference. As mentioned, sections have been noticed to become up to 50% thinner,[4,36] in the collection of tilt series data. If thinning takes place gradually during the collection, the reconstruction operations will severely fail, owing to unrestrained distortions of structures. The noise is more marked especially in thick sections than for whole mounts. However, thin sections also become thicker at high tilts (twofold at 60°)[52] and images are blurred.

The advantage with the sectioning technique, however, is that most material can be embedded, sectioned and structures of interest selected that would otherwise be difficult to isolate or are too bulky to study as whole mounts.

Standard fixation methods used in EM are usually inadequate for chromosomes and nuclear structure studies.[8,22] The fixation and staining methods that we have found applicable for section studies of chromosomes and nuclei are based on using RR in different combinations with GA, OT and, in dehydration before embedding in plastic resin, with UA (stain) in MeOH.

The procedure is as follows.

1. Specimens are fixed in 1–2% GA in 0.1 M NC buffer, pH 7.0–7.4, or in Ringer solution (RS), with (a) RR (750–1500 ppm) or (b) without RR, at RT, for 1–2 h or longer, washed in the NC buffer or RS.
2. Further fixed in 1% OT in the 0.1 M NC buffer or RS (2–4 h), RT, (a) with RR (750–1500 ppm) or (b) without RR, washed in the NC buffer or RS.
3. Stained in 0.1 M NC buffer or RS, (a) with RR (750–1500 ppm) or (b) without RR, for 24 h, at +4–8 °C, washed with buffer solution, briefly in water, before gradual dehydration in MeOH, then stained in 1% UA in MeOH [overnight (o/n) to several days, at +4–8 °C], washed in MeOH, transferred to absolute ethanol, propylene oxide, and finally to propylene oxide–Durcupan ACM (1 : 1), o/n.
4. Embedded in Durcupan ACM, epoxy resin (Fluka).

Controls: without RR, and with RR in the different steps and combinations.

The penetration of RR into nuclei and chromosomes can be checked in semithick section for phase-contrast LM.

Sections are cut with an ultramicrotome and mounted on grids according to standard EM thin-sectioning techniques. The sections on the grids are stained with Reynold's lead citrate (10–30 min, in a Petri dish with solid KOH to avoid precipitation), washed with freshly boiled FddH_2O and AD before examination in TEM.

Comments: importantly, to enhance the intracellular contrast with RR, it is to be used after the OT fixation (step 3). This is because OT fixation will destroy the semipermeability of cell membranes and RR will then penetrate and stain nuclei and chromosomes. Before OT fixation the intracellular penetration of RR is almost nonexistent. However, if high contrast is required, after staining with RR (step 3), postfixation with OT is added.

To study, e.g. interphase chromosomes, whole mounts of nuclei are too thick for ordinary 100–120-kV TEM. Thin sections must be used to collect the tilt series. Section thickness is, however, limited to <0.1 μm for 100–120 kV.

If thick sections must be used to incorporate spatial details, the embedding medium can also be removed. The sections are therefore changed to a kind of whole mounts. This improves the signal-to-noise ratio and makes the thick embedded material more permeable to electrons.

The material is fixed only with GA, before embedding and sectioning, and after removing the embedding, brought stepwise to buffer solution and prepared as whole mounts (section 2.4) or then processed as in bulk embedding for sectioning, i.e. fixed, stained, embedded and sectioned using standard fixation with GA or OT, or using the RR methods for chromosomes and nuclei, as presented above.

Gold markers are introduced only on the section-free side of the grid, to ensure that they do not float off when the embedding medium is removed. It may also be advisable not to poststain the sections with, e.g. Reynold's lead citrate, that may form precipitates when the embedding medium is removed. The procedure for dissolving the embedding medium from sections is somewhat different, depending on the different embedding media used.[62,63]

Removal of resin from ordinary epoxy thin sections is carried out as follows:[62]

1. Preparation of the solution: prepare a solution of seven pellets of KOH in 100 mL of absolute ethanol (the color of the solution will be light orange–brown when ready, after 1–2 days).
2. Immerse the sections (0.25–0.5 μm or thicker), mounted on carbon–Formvar grids, in the solution for several minutes (to be time tested, depending on section thickness and epoxy resin used).
3. Wash in ethanol and MeOH, with several changes.
4. CPD (section 3).

If section material seems to be lost, PL-coated grids (section 2.2) are used to ensure better that the material will stick to the grids.

Note that the method seems to be mild enough to be used with immunological methods.[62]

In addition, for enzyme digestions a method has been introduced[32] for immunostaining, e.g. interphase chromosomes. Isolated whole cells are encapsulated in agarose microbeads for the enzyme digestion and immunostaining procedures. Thick, resinless EM sections are obtained that are excellent for ETM purposes (applications in sections 2.3 and 7).

4 DATA COLLECTION

4.1 Recording of Tilt Series

Images recorded in TEM are two-dimensional (2-D) projections of a 3-D object. Owing to the large depth of focusing in TEM, all the details are usually in focus and superimposed in thick preparations, whole mounts and sections. Chromosomes lack symmetry, the kind of which is characteristic of icosahedral viruses. Thus, for 3-D reconstructions with ETM, single-axis recording of tilt projections is accomplished that after the alignment procedure is processed with the WBM and MEM.

A conservative prediction[52] of the resolution (d) obtained with single-axis ETM is correlated with the number (theoretical) of projections (N) available (from 0 to ±90°) and the object thickness (D), and is given[4] by Equation (1):

$$d = \frac{\pi D}{N} \tag{1}$$

The actual resolution realized is, however, difficult to estimate, as the number of projections is limited by the tilting range from 0 to ±60°. This tilting range is obtainable with standard specimen holders and goniometers in TEM. Special specimen stages and holders have been available earlier[64] and recently introduced for cryo-EM, including new rectangular grids.[65] Such grids with a 'grill-like' pattern have long been available, but the new 'cryo-tilting grids' are in a way improved because of the square shape, with rectilinear rims perpendicular to the tilting axis that will free the tilting procedure from shading grid bars. The disadvantage with these new grid holders is that there is no way of rotating the grid specimen. The rotation of the specimen is most important for oblong whole-mounted structures such as

chromosomes to orient them parallel to the tilt axis to record tilt series with optimal resolution in ETM.

4.2 Manual Recording

Although manual recording of tilt series in axial ETM will in the future be replaced by automatic recording (section 4.4), there are probably few laboratories today that have access to or can afford digitally controlled TEM equipped with automation facilities. Manual collection of tilt series is, after some training, a fairly quick procedure when recorded on EM photographic film plates [actually a faster procedure than recorded manually or automatically with a slow-scan charge-coupled device (CCD) camera]. The EM plates also have the advantage that the recorded area is very much larger than that covered by a CCD camera, and owing to this advantage for film plates, more and larger structures can be collected at higher magnification. This may be important not only for the structures under investigation but also for collecting gold markers for the alignment procedure, as there may not always be enough markers available in the area that the CCD chip covers. Manually, increments of less than 3° are difficult to accomplish in practice. We have found in any case that tilt series, from 0 to ±60° with a 3° increment, are sufficient for ETM reconstruction of whole mounts, and have become a standard for us. Testing tilt series, recorded with a 2° increment, has not shown significant improvements in reconstructions. However, reconstructions with a 5° increment give significantly less satisfactory results (however cf. Figure 1f, g, h).

Manual recording of tilt series is carried out as follows:

1. Check that the TEM is under optimal conditions, especially for 100 or 120 kV, which might differ from alignment settings at 60 or 80 kV.
2. Preferably, use a rotating grid holder, to adjust that the tilt axis is oriented optimally, i.e. along the length of the chromosomes.
3. Test, at low magnification, that the tilting from 0 to ±60° is attainable and not hidden, e.g. by grid bars. It is not absolutely necessary to cover the whole tilting (lacking one or even two images will not be a disaster).
4. Importantly, test that the preparation is stable, i.e. will not drift significantly during the recording. The stabilization can be improved by slight evaporation of additional carbon on grid specimens or by keeping the specimen in the electron beam, at low magnification, for some time (e.g. 5–10 min). If nothing helps to stop the movement, choose another place on the same grid for a new object, or change for a new grid specimen. Unstable specimens will easily ruin a reconstruction by blurring the whole or a great part of a tilt series. Restoring blurred images for high resolution with image processing is difficult, laborious or impossible.
5. Choose preferably the largest objective aperture, especially for whole mounts to achieve a high transparency, and a suitable magnification. According to our experience, the highest magnification with which we can collect a tilt series without significant radiation damage is about 60 000×. The electron beam must be kept as weak as possible to avoid radiation damage to the preparation. If possible, use the 'minimum-dose focusing procedure' that is available in some microscopes. This may be very useful for sensitive samples especially at high magnification.
6. A eucentric goniometer is preferable for collecting tilt series. The eucentricity of the goniometer must be adjusted as accurately as possible to be of use in collecting the tilt series. If goniometer adjustment is completed the specimen will not move and focusing will not change significantly, at least at low magnifications, when the specimen is tilted within the medium tilting range. Adjustment of the goniometer is, however, not very reliable, especially at high magnifications and tilting, and the focusing and shifting must usually be readjusted. If focusing must be corrected and if it is important to keep the magnification for each image in a tilt series unchanged, the focusing is adjusted with the *z*-control screw of the goniometer and by shifting the specimen back to position. If focusing is adjusted in a normal way during tilting, the magnification of the images will change. However, this incident will usually not be of much significance as most ETM programs will correct the scaling, i.e. magnification of each image, in the alignment procedure (section 5.1).
7. Collect the tilt series starting from 0 to ±60°, with e.g. a 3° increment (our standard). Some instructions[52] recommend starting from one extreme tilt end and move through zero to the other tilt end, to avoid sudden jumps in data collection that may occur owing to insufficient precision of the goniometer.
8. It is advisable to adjust the exposure parameters for photographic EM plates so that the plates can be developed with a machine (e.g. Kodak, used for autoradiography films) available in most laboratories. With this procedure, a check of tilt series is rapidly accomplished, so that negatives with faults, not in focus or missing can be replaced while the specimen is still in position in the microscope.

4.3 Digitalization of Photographic Negatives

Digitalization, i.e. scanning of the tilt series, is necessary for computer processing. Scanning is a more laborious

procedure than manual collection of the tilt series data on photographic negatives. At present scanning is also largely manual. According to our knowledge, there is no scanning device available with automatic feeding of EM plates to the scanner. However, devices for 35-mm film strips and also framed slide pictures can be fed and scanned automatically but not film plates of the size used in EM (e.g. 6.5 × 9 cm).

One of the advantages with EM photographic plates, as mentioned, is the large area of the specimen that can be recorded. This may partly compensate for the tiresome scanning work, in comparison with the limited view covered with a CCD camera. In addition, there are more working prospects with film plates, as they can be scanned with the resolution needed and they allow the choice of other sectors of interest, on the large plates, for scanning and with, e.g. higher resolution.

Ordinary flat-bed scanners (e.g. Umax PowerLook 2000) that we use today have a maximum resolution of 1000 dpi (in both directions, optical and mechanical), i.e. a pixel size of 25.4 μm. Better but also much more expensive scanners are available, e.g. drum scanners, but the manual scanning is much too laborious (attaching many negatives on the drum) for the improved resolution. A high-precision flat-bed scanner (Zeiss, Scan1) is available that has a pixel size of 7.5 μm (precision 2 μm), but the price is much more than 20–30 times that of an ordinary flat-bed scanner.

At a magnification of a negative of, e.g. 50 000×, scanning with 1000 dpi, the pixel resolution in the negative will accordingly be about 0.5 nm. This pixel resolution will exceed the conservative estimate of the resolution achievable, of ca. 5–8 nm, for an object with a diameter of, e.g. 100 nm (with 3° increments), according to Equation (1). However, the actual resolution frequently experienced is better than the conservative theoretical estimate.[52] In theory, the resolution that is achieved, is sufficient for twice, or owing to the many procedures in the alignment, 3–4 times the original pixel size.[52] Thus, oversampling with a 2–4 times smaller pixel size is of advantage for achieving in practice a needed resolution. As the grain size for EM photographic plates is, after chemical development procedures, estimated to be about 5 μm, this will in any case be the limit to the resolution that can be extracted from photographic negatives with digital procedures.

Scanning of the photographic negatives is carried out as follows:

1. Before scanning, dust from the negatives is removed with a soft brush, along with gentle breathing on the negatives, which will help, when the humidity is not high enough, to remove static electricity that might be a problem in dry conditions.
2. Up to eight negatives (size 6.5 × 9 cm), with shiny side down, are positioned on a flat-bed scanner (e.g. Umax PowerLook 2000).
3. The scanning is accomplished with a semiautomatic procedure together with automatic correction of contrast, of histograms, gamma values, etc. for each negative. Manual correction will take longer and the results will not necessarily be better.
4. The area and resolution (1000 dpi, optimal) are selected for the negatives and the title number for the image (corresponding to the tilt angle) and format used (e.g. jpeg) are recorded. The program automatically collects the data of the regions, according to the mentioned settings for each negative, in sequence.

Today, even with the advantages of semiautomatic scanning procedures, the completion of the scanning of all (e.g. 41, 3° increments) plates will usually take longer than the manual collection of the tilt series with TEM.

4.4 Automatic Recording

The automatic collection of tilt series data[40] will in the future replace manual recording methods. Automation is the only manner for very sensitive specimen recordings such as cryo-EMT procedures (section 3.4), which involve embedding in vitreous ice, as the exposure to the electron beam is reduced 10–100-fold, as mentioned. Automated low-dose data collection of a tilt series uses adjacent areas for correction of changes in image shift and focus. The selected area chosen for the tilt series is recognized with the cross-correlation function process. The images are recorded using a high-performance digital camera system, i.e. a cooled slow-scan CCD camera (1024 × 1024 or 2048 × 2048 pixels).[40]

Because of the cost, most laboratories will not have access to such facilities in the near future. However, to improve the resolution in ETM reconstructions, tilt series with smaller increment values are needed, e.g. 1°. The collection of tilt series with 1° increments is for practical reasons only possible with automatic data collection in digital format. Regardless of the preparative methods used, specimens suffer less radiation damage with automatic recording. In addition, the recording of the dynamic gray-scale range and avoiding image distortions are claimed to be superior with a CCD camera, in comparison with photographic film recording. All these improvements involving automatic data collection procedures are dealt with in a recent review.[40]

5 ELECTRON TOMOGRAPHY METHODS

5.1 Alignment of Tilt Series

The tilt-series images collected must be most accurately aligned to be sufficient for ETM reconstructions, especially after manual recording and scanning procedures. Alignment of the tilt series can be accomplished without markers by using the cross-correlation function method as used in the automatic data collection process. However, before the cross-correlation or other automatic method has been better refined, the use of fiducial markers has proved to be a more accurate method for the aligning of tilt series data.[4] A semiautomatic method is available, part of the program IMOD,[66] for fiducial gold marking with the advantage that some gold tags may not need to be present in all the images. However, at first glance, the method appears more complicated than manual methods in use.

As mentioned earlier, different-sized colloidal gold particles on the grids are convenient for different magnifications. The minimum number to be marked is three (or four[52]), ideally 10–20. Corresponding gold particles must be identified on all images of the collected tilt series, and preferably evenly distributed around the object to be reconstructed. Commercial gold markers are preferred, e.g. immunogold, as they appear to be more uniformly round (U. Skoglund, Karolinska Institutet, Stockholm, Sweden, personal communication) than laboratory-made markers.[67] The spherical form is important, as the program searches the midpoint pixel of the gold as the target for coordinates registered. Nevertheless, the search parameters can be turned to a minute search area to respond to manual correction, if an automatic search does not give the appropriate exactness. If sufficient gold particles cannot be found, other naturally appearing granules, etc. are usable as alternative markers within the area, only to be tracked accurately enough. It may be useful to add that in the program we have developed, the gold particles can be situated on any side or level on the grid. They need not to be on the same plane.

Our program, JPEGANIM for SGI machines,[28] used for the procedure has been appropriately designed for convenience, using interactive graphic interfaces with menus. The images of the whole tilt series are run as a movie, so each image can be sequentially viewed, back and forth, for rapidly recognizing the same gold particles in each image. The images can be contrast-enhanced temporarily or permanently, enlarged and moved to different regions when the image size exceeds the display, and processed otherwise, e.g. with unsharp masking and other filters. All these features aid in making the search and gold marking an easy and rapid operation.

When sufficient markers have been picked up and the files saved, the next step will be to test the alignment accuracy, using SOLVE from the menu in JPEGANIM. The program uses a conjugate gradient method that gives a set of overdetermined nonlinear equations that can be solved.[28] After running, the program produces a plot with evaluation of alignment correlation, in pixels, with estimates for all images and gold markers used, as graphical scores. The refinement is accomplished, when necessary, by either removing the worst gold markers, in sequence, or trying to correct the position of poor gold markers in the images with the poorest scores and rerunning the program. A set of files is used in the next step for an evaluation, which includes corrected tilting angles, scaling, midpoints and the axial angles.

The alignment procedure will then be tested with ALIGN from the menu, e.g. on a small area with only one, or a few, gold particles. A midpoint is chosen and an area framed with the mouse, producing a sequence of pictures. The z coordinate for the midpoint is obtained by using the parallax method, i.e. marking the same point from two image tilts, the zero and an end tilting image, for the best accuracy. If the same point is difficult to mark in the endmost tilt, any other image can be used. An area is then framed for the object to be aligned, from the midpoint, and the program will produce a set of aligned images, twice the size of the frame chosen.

After running the program, the accuracy of the aligned images can be tested as a movie. The movie must run smoothly and keep the midpoint in place, to obtain an accurate reconstruction. Scaling, rotations and translation of the origin are all corrected by the program.

With the test procedure adequate, the object for reconstruction framed and aligned images saved, there is saved a file including the size of the object, in pixels, with corrected tilt angles and a filtering parameter used in the reconstruction procedure. Occasionally, if a set of aligned images show sudden jumps at certain places, the corrected tilt angles are replaced with the original angles chosen, i.e. ideal values with the increments for the tilt series. (Direct goniometer readings are more precise than computed values.) A realignment (2–3 times) procedure of aligned images may also be of help in correcting the alignment for difficult tilt series.

The aligned images can be viewed in stereo mode. Gold marking in stereo can be of great help for identification in difficult circumstances. The stereo mode is also most useful in the examination and interpretation of the original EM images as stereo movies, involving image processing, contrast and filtering procedures for comparison with the 3-D reconstructions produced with ETM.

5.2 Reconstruction Methods

The ETM reconstruction programs that are used need a set of accurately aligned images, i.e. Radon transforms. The aligned projections must be twice the area of the object region selected and, as mentioned, this is accomplished by the alignment program, to be implemented for an ETM 3-D reconstruction of the object.

A reconstruction is first produced, as a test, with the WBM, a quick procedure in SGI machines (Origin 2000, 128 R12k processors, 160 Gbyte RAM). If the reconstruction with WBM shows adequate results, the reconstruction is completed with MEM. Today we use COMPAQ AlphaServer 8400, eight EV6 processors, 12 Gbyte RAM. This is advantageous, as ETM with MEM is calculation intensive. (An earlier approximation, to compare the time taken by the programs to complete a reconstruction of a certain volume, was the following: WBM took the same time in minutes as MEM in hours. However, this match is not very valid for long, as the computers are steadily upgraded, and now the time needed for MEM processing is less than half of our earlier estimate.)

5.3 Weighted Back-projection Method

For some reasons, the programs available for ETM [e.g. IMOD (URL: http://www.soapdish.colorado.edu/imod/download.html) public domain program and SPIDER & WEB (URL: http://www.wadsworth.org/spider_doc/spider/docs/spider_license.html) by license] use WBM processing for ETM reconstructions. This may partly be due to earlier limits in computing capacity. Another reason might be that WBM[36] has a long traditional line going back to Radon (1917).

In practice, our program (Backproject) does not need very much attention by the ordinary user and the reconstruction, once the filtering parameter has been determined, is an automatic procedure. The filtering parameter may be varied for an influence on resolution, smoothness or noise level of the reconstruction. However, in optimal cases, the appearance and resolution might be improved, but real improvements in reconstruction are more affected by the original quality of the tilt series and accuracy of the aligned images.

After developing and acquainting ourselves with the MEM procedure, we are now using WBM only as a rapid scrutiny method having in fact rejected WBM as a reliable reconstruction method. It is therefore unnecessary to go into the theoretical contents of WBM, as they have been presented earlier in detail.[28,36]

5.4 Maximum Entropy Method

The MEM was first introduced in an astrophysical context for filtering telescope pictures from noise, and the method initially presented significant improvements in image quality. The introduction into 3-D reconstruction procedures in structural biology was accomplished for the first time for chromosome studies, as earlier mentioned.[43] After this initial work, relatively few investigators in ETM have shown an interest in using MEM. This must be partly due to a lack of computing power and long processing times, or to poor evaluation methods used in viewing 3-D reconstructions.

In cooperation with Juha Ruokolainen (CSC, Center for Scientific Computing, Espoo, Finland), we decided to develop a MEM version of our own that was ready in early 1995. Later we extended our MEM also to a 16-bit MEM version that uses aligned 16-bit gray-scale images.[68] We became intensely aware of the need for better 3-D quality when we recognized the relatively poor accuracy of the WBM reconstructions viewed with the high-quality stereo procedures for ETM that we had developed earlier.[28]

MEM yields uniformly better reconstructions than WBM (cf. e.g. Figure 1f, g, h with Figure 5a, b), especially for whole-mount samples of chromosomes: they appear distinct in stereo viewing of the object with the volume visualization programs BOB and FUNCS (section 6.1). In addition, the noise level in WBM-reconstructed objects, as measured by α-values, is often as high as 100 or more (of the 256 gray-scale levels) when using BOB or FUNCS. With MEM the α setting is much less, often close to zero.

Another way of comparing the quality of WBM and MEM reconstructions is to examine the shape of gold markers. With WBM the missing data wedges between 60 and 90° stretch structures along the electron beam (z-axis). According to the results, MEM corrects errors due to missing data more effectively than WBM, and the gold markers are clearly less oblong with MEM.

The disadvantage with MEM is the long calculation time needed for large volumes (e.g. $400 \times 400 \times 500$ pixels), only manageable for laboratories having access to supercomputer facilities. However, even desktop computers are today as fast as yesterday's supercomputers, so it should not be long before any laboratory will have the capacity to perform such computing. For smaller volumes (e.g. $100 \times 100 \times 100$ pixels) with an ordinary desktop computer this might already, or soon, be possible within a reasonable performance time.

A description of our MEM deconvolution is as follows.[68] Solution of the deconvolution with MEM aims to minimize the function that is composed by the square of the reconstruction error (Equation 2):

$$e^2 = \|\rho - Af\|^2 \tag{2}$$

where ρ is the images and A is the back-projection operator, and by the regularizing term. The regularizing term in MEM is the entropy of the object to be reconstructed (Equation 3):

$$E = -\sum_i \sum_j f_{ij} \ln f_{ij} \tag{3}$$

where $f_{ij} = f(x_i, y_j)$ is the object to be reconstructed. The quantity f must be positive. Combining Equations (2) and (3), the problem may now be presented as an optimizing problem: search for f_{ij} such that the expression $\mathbf{A}$ is at minimum (Equation 4):

$$\mathbf{A} = \sum_i \sum_j f_{ij} \ln f_{ij} + \lambda \|\rho - Af\|^2 \tag{4}$$

where A is the Radon transform operator representing the reconstruction function as back-projections of images. The Lagrange coefficient, λ, is a regularization parameter, which weights the reconstruction error with respect to the entropy.

As mentioned, the experiences with MEM are promising. For example, noise is notably eliminated, and so is the waving that the Fourier transformation also causes. In addition, according to the definition, MEM produces a positive reconstruction of the object, in contrast with the Fourier transformation method. The density quantity should be positive. Additional MEM deconvolution procedures can be found elsewhere[36,43] and in a recent application.[41]

Our MEM procedure (MaxEntropy) is almost as transparent for the user as WBM. In the file that is created in the saving of the aligned images, the regularization parameter is added after the filtering (default) value. If problems appear, often seen as regions of minor stripes or bands, then this regulating parameter is tested with other values until the reconstruction has been refined to remove the minor distortions.

There is an additional regularization parameter for our 16-bit MEM. This 16-bit MEM, as yet not much used, will be especially useful when 16-bit gray-scale images are accessible with high-performance 16-bit CCD cameras with automatic data collection of tilt series, especially in cryo-ETM procedures.

As already mentioned, MEM is executed on a COMPAQ AlphaServer (8400) SG 140 (eight processors, 12 Gbyte RAM), especially for large volumes. However, the data have to be converted to be usable for viewing the volumes in the SGI machines, as the bytes in the Alpha machines are in a different order. This inconsistency is corrected by using a conversion program in the Alpha machine to make the volumes applicable for SGI machines.

Actually, a set of different conversion and other subprograms are repeatedly used. There is no reason to go into all the details, as different programs and machine set-ups may require different modifications.

5.5 Dual-axis Tilting Method

In conventional single-axis tilt series, the tilts used are limited to the range from 0 to $\pm 60^\circ$. As already mentioned (section 4.1), grid holders are available for increasing the tilting range, e.g. from 0 to $\pm 70^\circ$ (or even up to 80°), but at the highest tilting ranges occultation easily occurs, and for sections the thickness will in general become too large, especially at very high tilts, e.g. two times thicker at 60° and three times thicker at 70°,[52] for collecting reliable data with conventional 100–120-kV TEM.

Methods have recently been introduced to reduce the missing data wedge, e.g. between 60 and 90°, by using dual-axis tomography tilt series,[69,70] The two programs transform the missing wedge to a missing pyramid, and combine somewhat differently the two orthogonal single-axis tilt series obtained by 90° rotation.

The dual-axis tilting approach has shown improvements in some situations, e.g. membrane vesicles appear restored from distortions in comparison with the single-axis method. Detailed instructions on the procedure, with or without a specimen-rotating grid holder, have recently been prescribed.[52]

It seems doubtful if any improvements can be obtained for oblong structures such as chromosomes and chromatin fibers, as microtubules oriented perpendicular to the tilt axis fade and are lost in reconstructions.[52] In any case, improvements have been claimed, at least in some cases, also for microtubules.[70] According to our experience, long structures, e.g. microvilli, when tilted perpendicular to the tilt axis, appear very unsharp and faded along the reconstruction. It is obvious that the dual-tilting axis method is useful only for fairly rounded objects that need not be specially oriented for collecting tilt series.

In our experience, to test cryo-preserved preparations (in cooperation with H. Cheng, Karolinska Institute, Stockholm, Sweden, and M. Marko, Wadsworth Center, Albany, NY, USA) using our MEM procedure and combining the dual-axis tilt reconstructions with IMOD,[70] no clearly distinct improvements emerged. However, all possible refinements have not yet been accomplished and the original tilt series from the sections used were, for some unknown reasons, difficult to align accurately. Such inaccuracies may have contributed to the unsatisfactory result, as the improvements usually detected with a dual-axis tilting method seem to be the most delicate[70] and advantageous when all basic parameters are refined to the optimum.

6 RENDERING OF RECONSTRUCTED CHROMOSOMES

6.1 Visualization of Three-dimensional Reconstructions

When a chromosome reconstruction has been completed with WBM or MEM, there are several ways to visualize 3-D volumes. In any case the reconstruction must be in the right format for the program. For such conversions another set of programs are used.

As indicated, we regularly use two programs for SGI machines, BOB (a public domain program, University of Minnesota, Graphic Visualization Laboratory, Army High Performance Computing Research Center) and FUNCS,[28] that efficiently display volumes of 3-D reconstructions of, e.g., chromosomes in stereo mode.

The SGI workstations (Octane, 1 Gbyte RAM, and Onyx2, 4 Gbyte RAM with 4 MIPS R10000 processors and InfiniteReality2E-graphics), with high-frequency displays, and provided with liquid-crystal stereo (Crystal Eyes) eyeglasses, synchronized by an infrared light device controlled by the computer, show images in color stereo mode. According to our experience, stereo viewing is the only way of even beginning to comprehend the geometry and 3-D structure of chromosomes (Figures 1f, g, h, 8a, c, 9a, b and 10b, c). Other methods might involve

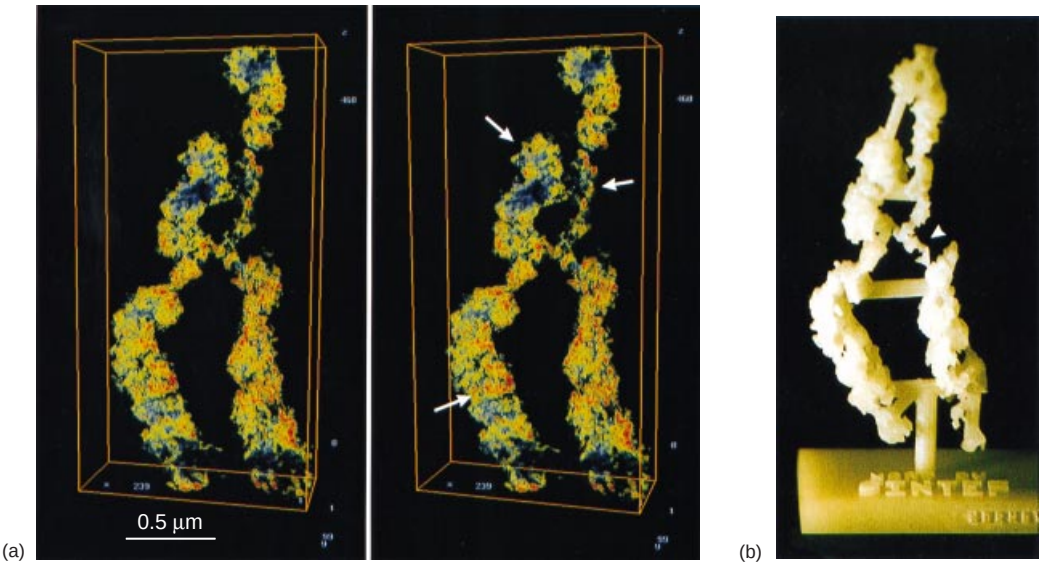

Figure 8 (a) Chromosome scaffold, stereo pair of 3-D reconstruction with MEM, section 5.4. [AA-isolated chromosomes from HeLa cells, prepared as in section 2.4, procedure: 1(b) and (c), then treated as in section 2.3, with DNase and RNase digestion; then as in section 2.4, Procedure 1(d) and dried from *tert*-butanol, section 3.2.] Typical coiling appears in chromosomes, although they are depleted of histones and DNA, showing that scaffold elements are maintaining the coiling. The pattern and structures that can be detected are wholly in agreement with the unified loop-and-rosette chromosome model (Figure 1). The unified model gives predictions about the structure of the chromosome core regions, i.e. scaffold, in all details. Ring-like structures that are in agreement with the size of cyclomeres are detected (arrows) in the chromosome scaffold. In addition, gyres of the scaffold macrocoils measure to fit two rows of cyclomeres, e.g. in a zigzag pattern [cf. zigzag ribbon model for arranging nucleosomes in the 30 nm chromosome fiber[4,17]], although minor coils,[25] e.g. solenoid arrangement of cyclomeres, can also be seen closer to the centromere region, indicating that the structure of the chromosome coiling is versatile. (b) Hard copy, i.e. solid 3-D plastic model (section 9) produced earlier[28] from a WBM 3-D reconstruction. Coiling and many of the ring-like structures are found in the hard copy and importantly arch-like bends (arrow) that the unified loop-and-rosette model also predicts (cf. Figures 1b and 2c). (c) Immunoblottings with antibody (Ab) to H1 and H2b (antibodies to histones H1 and H2b kindly provided by Dr M. Bustin, NIH, Bethesda, MD, and Dr B.D. Stollar, Department of Biochemistry, Tufts University School of Medicine, Boston, MA, USA, respectively): 60% AA-isolated chromosome pellet, 60% AA-isolated chromosome pellet that has been further boiled (0.5–2 min) in 50% AA, and as positive controls the supernatant of 60% AA extract and of whole cells. LMW (low molecular weight) protein markers (Bio-Rad). Text in each sample column. (d) AA-isolated chromosomes fluoresce brightly with the DNA-specific fluorochrome DAPI. Digestion with nucleases DNase I and RNase A (section 2.3) remove all detectable fluorescence, but chromosome scaffolds retain their original shape and can be seen in LM (text in each picture). [(a–d) partly published in Engelhardt et al.[28,54]] (e) Stereo series of the chromosome scaffold arm [see (a)] with 10° increments around the tilting axis for each row, to observe the chromosome coiling from various directions. Ring-like structures of cyclomere size (arrows) are present. Thicker gyres (arrowheads) of the scaffolding coils seem to be fitted with two rows of cyclomeres in a zigzag pattern as suggested in the unified loop-and-rosette chromosome model [Figure 1, and cf. (a)]. [There is resemblance to intact chromosomes, with histones and DNA, having 'large-scale domains, roughly 100–130 nm in width', as described in EM tomographic sections of metaphase and telophase chromosomes by Belmont;[30] cf. his Figure 1.]

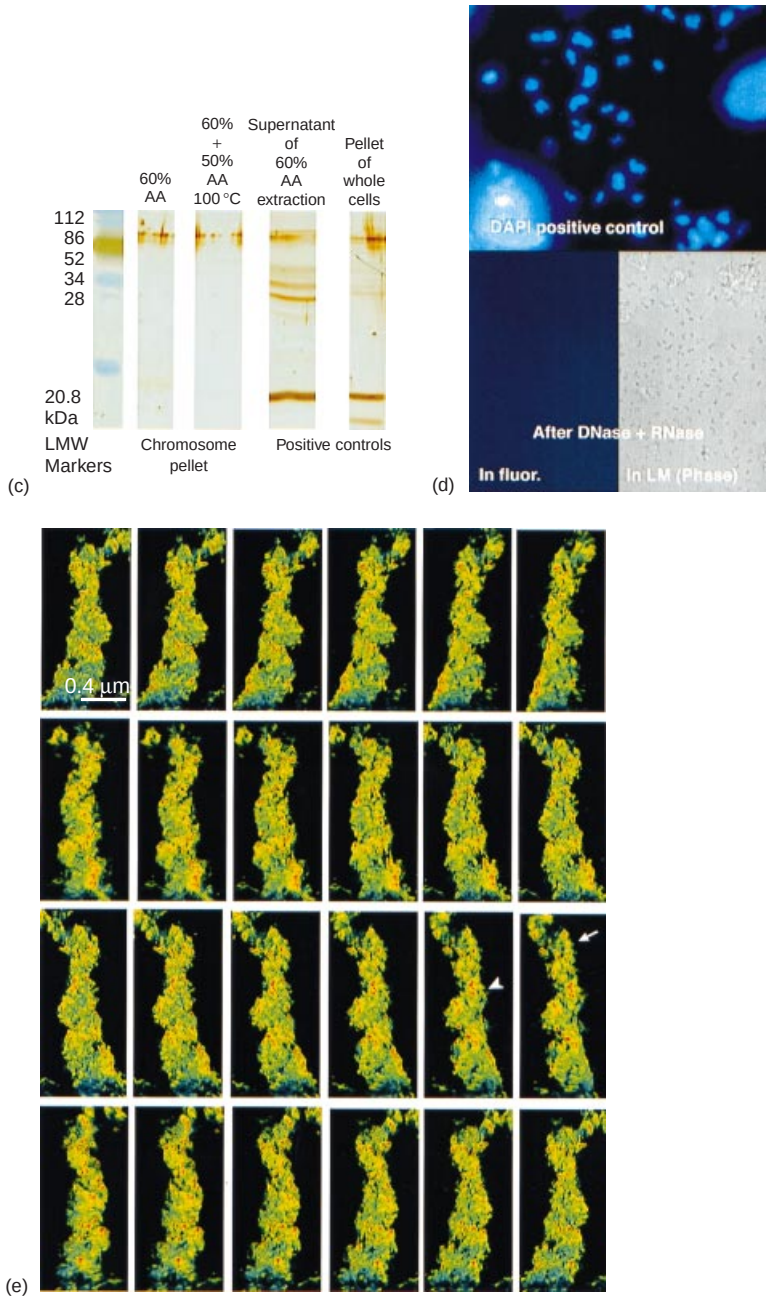

Figure 8 (*Continued*)

underestimation of the structural complexity and be rather pointless in really getting to grips with the 3-D reconstruction by ETM.

The 3-D reconstructions of chromosome are shown as translucent objects, regulated by alpha blending, and color may be introduced for different gray-scale ranges, composed of voxels, the size and density correlating with the pixel resolution of the original EM image projections. Viewed in mono and gray-scale, the reconstructed 3-D chromosomes look identical with the original 2-D EM images. Gray-scale viewing in stereo mode may actually be a more correct way to resolve complicated structures than replacing gray-scale values with various colors; although the colors look inspiring, they may actually confuse, not only beginners, rather than clear up complex structures. However, replacing gray-scale values with different colors can effectively intensify minute density differences for detection and analysis (e.g. Figure 9b).

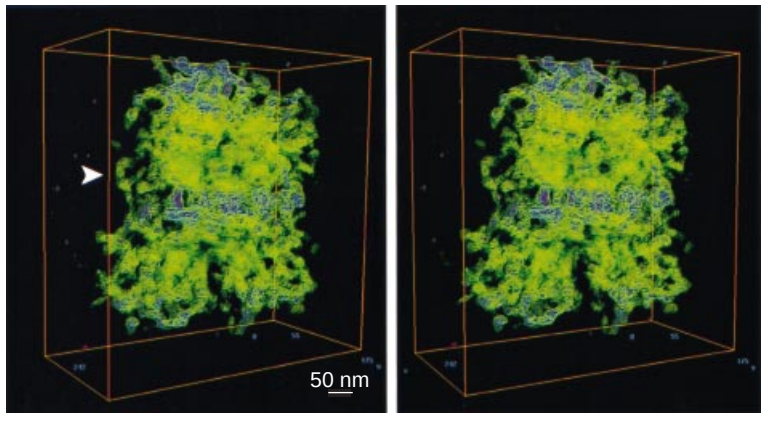

(a)

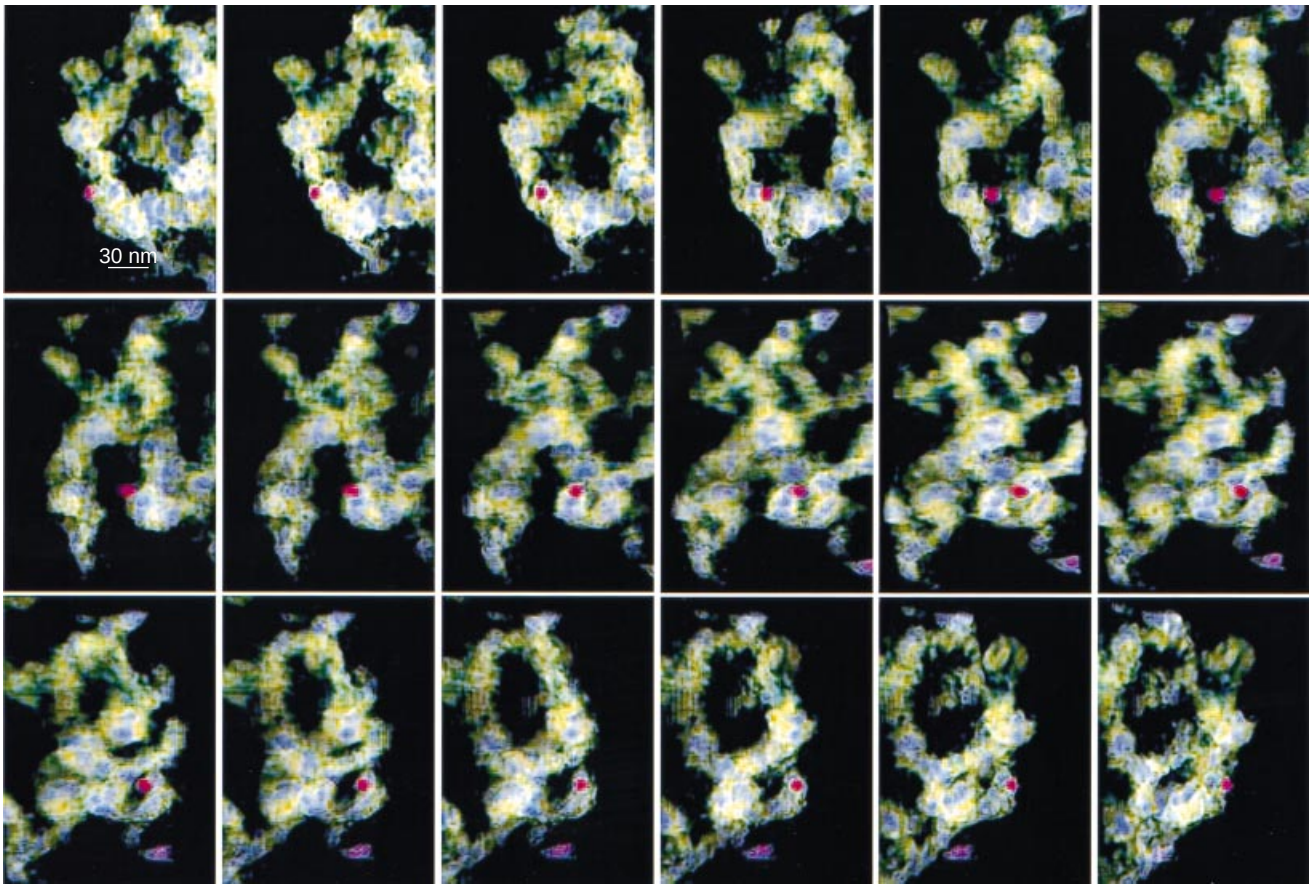

(b)

Figure 9 (a) Stereo pair of MEM 3-D reconstructed chromosome scaffold of a small (HeLa) chromosome (prepared as in Figure 8a) visualized with BOB (section 6.1; cf. Figure 1f). Coiling is obviously not prevalent in this size class of chromosomes, as it would require a certain length. However, scaffold fibers can be studied in more detail. Scaffold fibers appear as disordered fibers and arches or have an open ring-like form (arrow), as the loop-and-rosette model predicts. In the background fiducial gold markers (red color) are seen. [Reproduced from Engelhardt and Ruokolainen[54]]. (b) Detail from (a) (thick arrowhead), stereo series of scaffold fibers rotated along the tilting axis, with 10° increments. Along the fiber perforation-like structures are obvious (light blue). A 10-nm gold particle (red) is visible among the fibers. A description of the perforation pattern of the fiber structure has been presented earlier[54] as peripherally located toroid-like structures of about 8 nm in outer diameter with a central hole of about 4 nm, but also open toroids could be detected along the spirally wound scaffold fibers. It was suggested that the perforations (toroids) are manifestations of topoisomerase II (a main scaffold protein). [Stereo pair in (b) reproduced from Engelhardt and Ruokolainen.[54]]

Furthermore, a 3-D reconstruction can be rotated and moved in any direction, enlarged, sliced and details can be cut out for closer viewing, or joining of voxels can smoothly display large volumes.

We use the programs for different aims. BOB is an easy and fast way for regular viewing of large and small volumes in stereo mode. FUNCS is slightly more difficult to use, but includes more features, such as introducing different-colored lights from different directions, interpolation of volumes or showing the volume as surface view (isosurfaces). Most importantly, FUNCS allows high-quality animations (section 6.2).

Other methods, such as sectioning the volume from any direction into 2-D slices that can be viewed in series, as a slow or rapid movie, also in stereo mode, or from all directions simultaneously, are available for dissecting and analyzing reconstructions.[52] These and other features are found in such programs as IMOD and SPIDER & WEB (section 5.3).

6.2 Producing Stereo Animations from Three-dimensional Volumes

The problem, when viewing high-resolution reconstructions of, e.g. chromosomes, is that volumes (over $200 \times 200 \times 200$ pixels) become slow, i.e. scenarios have to be recalculated by the computer, e.g. when the image is enlarged or the direction is slightly changed, e.g. in tracking structures in detail. The recalculation takes time, relative to the size of volume, which causes difficulties in following details when minor structural changes take place, i.e. causes loss of the track.

New effective high-end SGI workstations (as detailed in section 6.1) are available that may solve the calculation problems at least up to some volume sizes. However, the programs have to be updated (rewritten) for new workstations.

A much simpler and effective way to solve this kind of problem, which we have used earlier, is by creating high-resolution animations[28] around an axis, usually the tilting axis (Figures 1g, h, 8e, 9b, 10c). These animations can be produced from any size of reconstructions that are recovered with ETM, including interpolations and illumination from different directions, both of which improve significantly the appearance of details. Animations are produced with FUNCS, around the tilt axis with, e.g. 10° increments and three-time interpolations. However, animations with smaller increments, e.g. 1–5°, improve the tracking of details considerably. Depending on the size of the volume, the animations are produced in less than 1 h up to o/n.

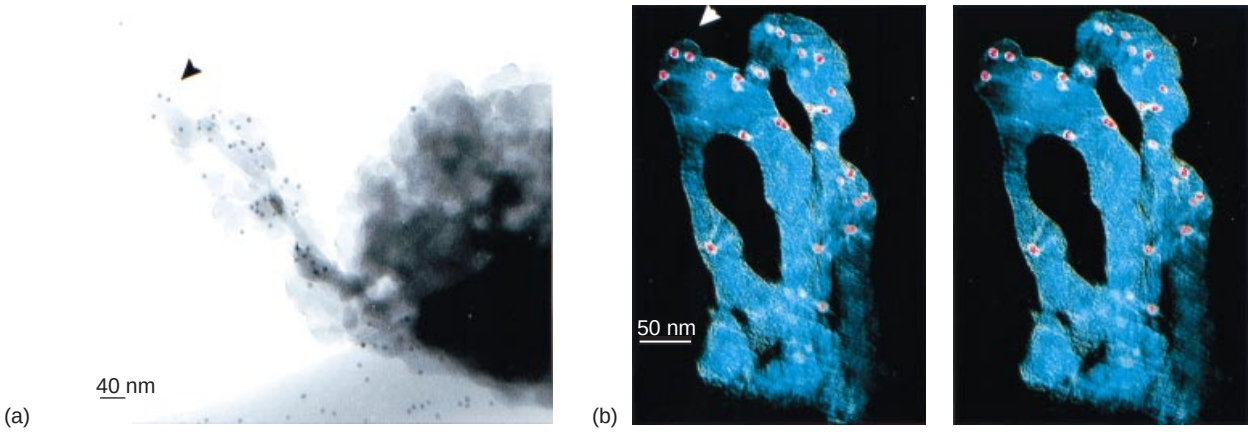

Figure 10 (a) Tilt picture (+45°) from the tilt series (0 to ±60°, in 3° increments) of chromosome scaffold (prepared as in Figure 8a). Overhanging scaffold fibers are seen originating from the chromosome scaffold torn from the carbon–Formvar film, visible at the picture base with 10-nm gold particles. The freely dangling scaffold fibers were used for the 3-D reconstruction to achieve the highest resolution. After high-resolution scanning the pixel size corresponds to 0.4 nm in the tilt series, collected at 58 000× magnification. [Another tilt picture from this series published in Engelhardt and Ruokolainen.[54]] (b) Stereo pair of MEM 3-D reconstruction of freely hanging scaffold fibers. Fiducial 10-nm gold particles are seen tagged to the fibers. (c) Stereo series, with 10° increment, of MEM 3-D reconstruction of top part [arrowhead in (a) and (b)] of the scaffold fibers, from high-resolution animation series (interpolating pixel vs voxel size to 0.1 nm). In stereo, an impression is made of a slender mostly peripheral lace-like structure, demarcating sharply the scaffold fiber periphery. [Outer mesh diameter 3.5 nm, inner mesh diameter and thickness about 1.5 nm. These values are rough as they are on or below the limit of the 'conservative estimate of resolution',[52] which is about 3 nm, Equation 1.] Stereo viewing reveals that the gold particles are inside the stretched fibers. This confirms that the fibers are very empty indeed. If the lace-like covering is real it could be part or derivative of the NE lamina that has recently been shown to be found inside the nuclei with IEM[32] after DNase digestion. [Stereo pair of this series published in Engelhardt and Ruokolainen.[54]]

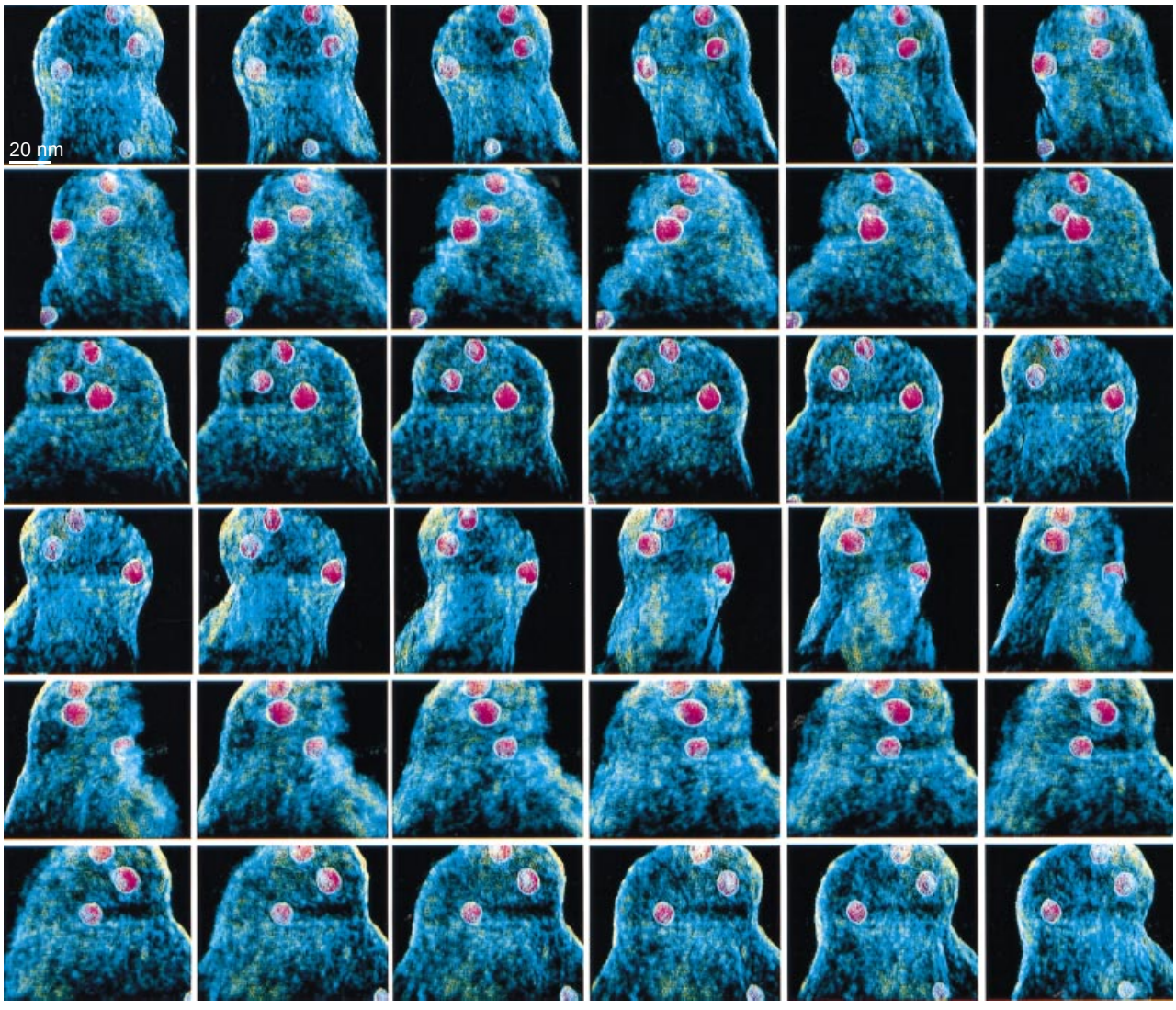

(c)

Figure 10 (*Continued*)

The images of an animation are saved in high-quality jpeg format and viewed with JPEGANIM, in stereo mode. Also, as already mentioned, from the menu of JPEGANIM, the movies can be magnified, moved to different regions, and structures can be measured with great precision, run with different speeds or very accurately by stepwise moving, smoothly, frame after frame. With these animations, the stereo viewing is not disturbed by blurring recalculations as the animations are sequences of ready-processed images that are all in the memory of the SGI workstation (as detailed in section 6.2).

6.3 Computer-aided Virtual Environment

Another means of 3-D visualization of volumes that we have recently used for viewing 3-D reconstructions of chromosomes, usable also for an audience, is the computer-aided virtual environment (CAVE) (available, e.g. at the Helsinki University of Technology).

The CAVE is a room, with wall-sized displays (three walls and the floor), controlled by a high-end SGI workstation (Onyx2, Infinitereality, 1 Gbyte RAM and four R10000 processors). High-end precision projectors, controlled by the SGI workstation, project the images of the volume on the walls. The viewers stand in the middle of the CAVE with liquid-crystal stereo (Crystal Eyes) eyeglasses. The rotating volume can be seen in 3-D form from all directions and from within at high resolution.

No doubt the 3-D view obtained is most impressive with very accurate details, as the whole volume is seen with all details and not limited by frames, as happens with

ordinary computer displays, when the object is magnified. The impression is that this is not only an excellent method for showing 3-D reconstructions for a group, to promote meaningful discussions among researchers, but also an important tool for perceiving structures that cannot be easily displayed in other ways.

7 IMMUNOELECTRON TOMOGRAPHY

The ultimate goal, in structural studies and particularly in 3-D reconstruction studies with ETM of biological specimens, would be to recognize different proteins, nucleic acids and other macromolecular assemblies straight from their structural 3-D configuration.

Before this ideal goal, achievable perhaps in the distant future, we have to use some other means of identification, such as immunological methods. Immunological methods work strikingly adequately in locating specific proteins at LM and EM levels.[67]

We have recently developed IET methods.[47] In principle, these methods do not differ much from ordinary IEM methods. We have used whole-mounted cells grown on EM grids for IET. Primarily, whole-mounted cells are not usually used in IEM in the way that thin sectioning or whole mounts of protein assemblies or objects of comparable size have been used. In whole-mounted cells or objects such as chromosomes, the immunolabeling would be difficult to distinguish because of the thickness and superimposition of immunolabeling in the 2-D images in TEM of such samples.

However, whole mounts are very suitable for IET. Instead of attaching gold markers on the grids for aligning the tilt series, immunogold labeling will be most adequate for the alignment. The different-sized immunogold markers will identify different proteins on the same preparations.

The problems in the development procedures were obtaining clean control preparations and preserving the cell ultrastructure, antigenic properties of the proteins and making cells permeable to immunogold labeling. In our IET reconstructions, we could easily see 5- and 10-nm gold conjugates. In addition, in distinct reconstructions, 1.4-nm immunogold (Nanoprobes Inc.) was detected especially clearly in overhanging microvilli, where the carbon–Formvar support had been torn away. This was to accomplish a set of high-resolution tilt series, so that the resolution was not obstructed by the support (Figure 11).

It remains to be seen how IET works for whole-mounted chromosomes, but we see no prominent difficulties. The steric hindrance by DNA present may cause penetration problems for immunogolds used. Thus, DNase-treated chromosomes, i.e. isolated chromosome scaffolds, would be the primary target in identifying scaffold proteins in 3-D reconstructions. The antigenicity of proteins may be hampered by 60% AA isolation of chromosomes, so that a more physiological method for chromosome scaffold isolation[19] might be immunologically more suitable. In any case, 60% AA-extracted histones had not lost their antigenic properties (Figure 8c) as shown in immunoblottings.[54]

IET procedures[47] modified for whole-mounted chromosomes are as follows. The starting material is chromosomes or chromosome scaffolds[19] mounted on PL-coated or glow-discharged carbon–Formvar–Ni grids[51] (section 2.2). The treatments are performed on Parafilms, with drop-sized depressions on wet filter-paper in Petri dishes (section 2.3). Washings and incubations are performed at RT, preferably on a tabletop shaker (gentle shaking). All solutions are filtered through a 0.22 μm (Millipore) filter. Small amounts that are difficult to filter are centrifuged, e.g. Ab mixtures, GA and OT solutions.

1. Prefixing in 0.125% GA in HM solution, 15 min.
2. Without prefixing:

   Wash in HM solution, several drops.

   Preincubation: wash and incubate o/n in TXHS (0.05% Triton X-100, 30 mM HEPES, pH 7.4, 0.1–0.5 M NaCl, 20 mM KCl, 5 mM $MgCl_2$, 20 mM glycine, 0.02% NaN_3), with (a) 0.5% fish gelatin (FG), or (b) no FG, 1–2 h at RT, and/or +4 °C o/n.

   (a) Incubation in primary Ab mixture (1 + 2):

      (i) Rabbit polyclonal Ab for protein 1 (LM-checked, e.g. $1:50–1:10^3$).

      (ii) Mouse monoclonal Ab for protein 2 (LM-checked, e.g. 1:25).

      Diluted in (a) TXHS + FG or (b) TXHS, 1–2 h at RT, and +4 °C o/n.

      Wash in TXHS, in several drops (1–10 min per drop).

   (b) Incubation in secondary gold-conjugated Ab mixtures; examples:

      (i) Mixture: goat anti-rabbit (GAR)–10 nm gold (1:25 dilution, Sigma) with GAR–1.4 nm gold (1:25 dilution, fluoronanogold, Nanoprobes Inc.) and goat anti-mouse (GAM)–5 nm gold (1:25 dilution, Sigma), diluted in (a) TXHS + FG or (b) TXHS, and/or

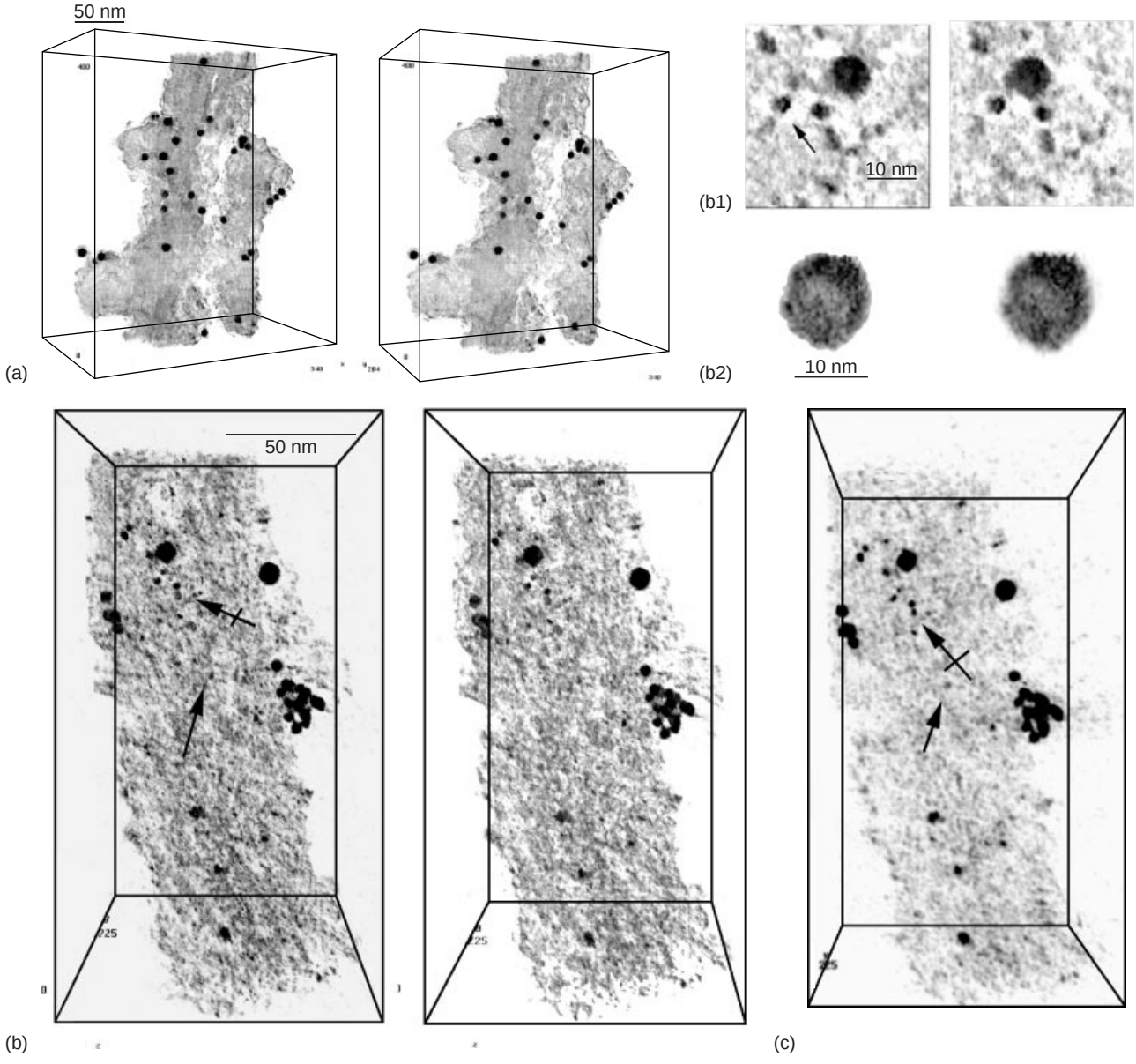

Figure 11 Examples of IET. Microvillar proteins in MRC-7 cells. Overhanging microvilli (without carbon–Formvar support) of MCF-7 cells,[47] will be representative samples of IET methods developed that may analogously be used for IET chromosome studies (section 7). (a) Stereo pair (BOB, cf. Figure 1f) of microvillar ezrin labeled with 10-nm gold particles. The specimen was postfixed with the GA, OT, TA method[47] (section 7). TA was used to minimize shrinkage of the samples after GA fixation (sections 2.4 and 7). The raw IET data (sections 4.2, 4.3 and 5.1) were processed with MEM (section 5.4). The 3-D preservation using TA shows more substructural details than without TA [cf. (d)]. (b) A stereo pair image [as in (a)] of microvillar ezrin and mucin. The specimen was postfixed with the TA method [as in (a)]. Ezrin was labeled with 10- and 1.4-nm gold conjugates and mucin with 5-nm gold conjugates. MEM 3-D reconstruction methods were used [cf. (a)]. Ezrin labeled with 1.4-nm gold particles is marked by arrows. Arrow with ribbon shows clusters of 1.4-nm gold particles. The intermediate-sized particles depict mucin labeled with 5-nm gold conjugates. (b1) Detail of (b) showing a stereo pair of 1.4-nm gold clusters (arrow) at higher magnification. (b2) Details in a single 10-nm gold particle. (c) IET reconstructed with WBM (section 5.3), for comparison of the same microvilli as in (b) with MEM procedure. Gold labels are seen but the 3-D reconstruction is less sharp and more noisy. (d) Stereo pair image [as in (a)] of MEM 3-D reconstructed microvillus as a control without TA (section 7). Ezrin was labeled with 10- and 1.4-nm gold conjugates and mucin with 5-nm gold conjugates. The 1.4-nm gold conjugates are present but more difficult to detect than in (b) with TA (presumably the detection of 1.4-nm particle size is more difficult owing to the shrinkage caused by GA fixation and CPD, which the treatment with TA seems to prevent.[55] [Reproduced from Engelhardt et al.[47]]

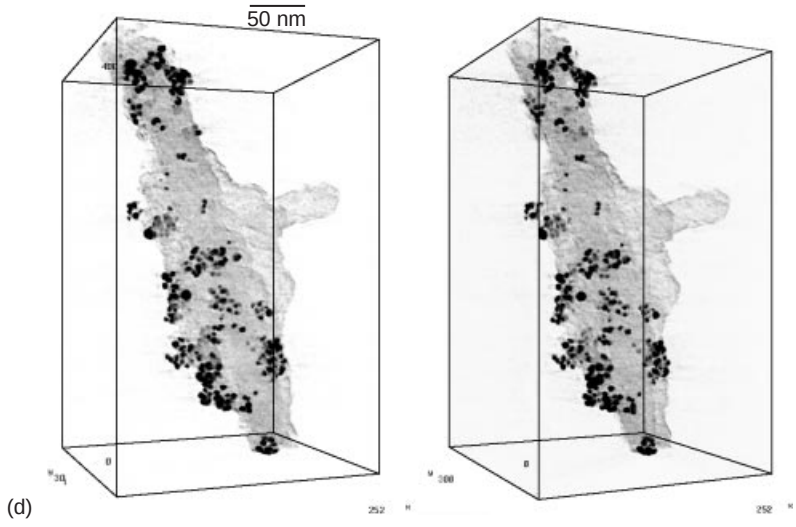

Figure 11 (*Continued*)

(ii) Mixture: GAR–10 nm gold (1 : 25 dilution) with GAM–5 nm gold (1 : 25 dilution) and GAM–1.4 nm gold (1 : 25 dilution), in (a) TXHS + FG or (b) TXHS.

Incubation: 1–2 h at RT and 4 °C o/n.

Wash in TXHS, several drops (1–10 min per drop).

Wash in HM, several drops.

3. Postfixing: 1.25% GA (1 h–o/n) in HM, (a) add OT (from e.g. 1% stock solution) in 0.1 M NC buffer, pH 7.4, to 0.3% OT as a mixture with GA in HM, 1–5 min, RT; (b) no OT.

   Wash in HM, several drops.

4. TA: (a) 1% TA in 0.1 M NC and HM (1 : 1), 5 min (for whole-mounted cells 1 h–o/n); (b) no TA.

   Wash in HM, several drops.

5. Dehydrated in 30, 50, 75, 100% MeOH.
6. Stain in 0.001–0.002% UA in MeOH (30 s), wash in MeOH.
7. CPD or other 3-D-preserving drying methods (section 3).

Controls: In IET controls, control (preimmune) serum was used or primary serum Abs were omitted and samples were postfixed only in GA (with or without TA), with no UA before step 7.

LM: immunofluorescence fixed in 3.5% paraformaldehyde in HM, using secondary GAR–fluorescein isothiocyanate (FITC) and/or GAM–Rhodamine, according to standard protocols,[51] mounted in DAPI/MM.

For immunolabeling of resinless thick sections, enzyme-digested or not, of whole-mounted cells, see section 3.5.

8 IN SITU HYBRIDIZATION ELECTRON TOMOGRAPHY

Analogous with IET methods, the same development concerns in situ hybridization electron tomography studies. In situ hybridization methods have been accomplished for EM earlier[67] and in microspreading of meiotic chromosomes, i.e. EMISH (electron microscopy in situ hybridization).[51] In principle the very same methods would be sufficient.

In addition, LM in situ hybridization techniques are standard procedures[51] only to replace, e.g. after the first biotin–avidin amplification procedures, the second one with gold-conjugated avidin, and replacing AD with, e.g. CPD (section 3).

FISH (fluorescence in situ hybridization) preparations are frequently contaminated with background signals that may be difficult to eliminate and spoil the accuracy required with in situ hybridization for EM preparations. In addition, cytoplasmic fragments regularly contaminate LM and microspreading preparations in EM studies.

It is therefore essential to strive for chromosome purification methods where cytoplasmic contaminations are eliminated, to be useful for in situ ETM. In addition, it is important to refine blocking methods to remove any background and unspecific labeling.

Superimposing contaminants and background labeling may disturb ordinary in situ hybridization EM preparations. ETM has the advantage that from the 3-D reconstructions, superimposed contaminating materials may be eliminated, as chromosomes with specific labeling can be cut out from surrounding material with ETM procedures and the pure 3-D chromosome reconstructions can be analyzed separately in detail.

9 HARD COPIES, PRODUCTION OF SOLID THREE-DIMENSIONAL MODELS

Hard copies, e.g. photographic prints, are produced of computer images, and hard copies of 3-D reconstructions of, e.g. chromosomes can also be produced, as we showed years ago.[28] This manufacturing procedure is called rapid prototyping technology (RPT). Today also the term laser stereolithography (laser photo-polymer technology) is used, including various other manufacturing procedures.

The solid 3-D model produced by the RPT method of our reconstructed chromosome scaffold is presented with all details. Our primary 3-D reproduction had to be supported by solid bars to maintain the spatial relationship of various parts. The material, from which the model is manufactured is nontransparent and somewhat fragile. The height is 13 cm and the width and thickness are relative to the computer reconstruction. Also, most of the details, although complicated, are reproduced with comparative accuracy that is limited only by the nontransparent material that is less useful for structural studies.

The technology to reproduce solid 3-D models of 3-D reconstructions is advancing rapidly. This will bring us solid 3-D models of more transparent material with different colors to accentuate, e.g. internal structures with the same density, i.e. isosurfaces. Such hard copies will be a great aid for complex structural studies that chromosome structures particularly require.

We must admit, however, that although the impression of the original chromosome scaffold appeared as a typical chromosomal coil, and the impression of a coiling structure prevailed in the viewing of the 3-D reconstruction in the computer, the solid 3-D model could neither verify nor disprove the coiling configuration.

Actually, we can realize that this apparent conflict may arise because the scaffold is not a uniform structure but is composed of thicker and thinner segments, i.e. coiling does not look very regular at a closer look. Owing to the irregular thickness, the coil appears also dually as sequences of bands and interbands, although the bands are actually just thicker clusters of the coiling scaffold structure and the interbands are thinner regions of the coiling scaffold, as the loop-and-rosette model predicts.

The higher level structure of chromosomes is indeed very complex. Neither the 3-D reconstruction (performed with WBM) nor the solid 3-D model allowed unambiguous structural interpretation of configurations. Further, the problematic situation of chromosome coiling (cf. Figures 1f, g, h and 8a, e) resembles the level of the 30-nm chromatin fiber.[4,17] Chromosome structures at all levels are much more complicated than we think and the methods are not yet sufficiently developed.

10 METHOD DEVELOPMENT

A program and instruments to collect tilt series automatically for ETM are now available. An accurate automatic alignment procedure, at least as accurate as the fiducial gold markers, would also be very useful. The two programs would constitute the all-automatic ETM kit. The system would use a supercomputer facility in connection with a computer-controlled TEM. Not too many obstacles are likely to be in the way of such a development. Whenever possible, the cryo methods would be used on unfixed and unstained specimens embedded in vitrified ice. The cryo-TEM techniques are fast and specimens are relatively easy to prepare and fully hydrated, i.e. close to the native state. However, the problem of noisy images in cryo preparations must be solved with filtration programs. We recently succeeded in eliminating at least partly the noise from some cryo-embedded preparations, with programs that we developed. The noise problem in cryo-specimens may thus be tractable.

A viewing room and facility, such as CAVE or VR (virtual reality) CUBE (Royal University of Technology, Stockholm, Sweden), will be indispensable for thorough analyses of high-resolution 3-D reconstructions.

With chromosome structure as an example, we realize that many structures are too complex for comprehension with present 3-D reconstruction methods, including hardware solid 3-D models. Thorough analysis with methods and programs may be useful, e.g. for tracking specified structures manually, semiautomatically or automatically, in 3-D form, from section to section. Such tracking studies on whole-mounted chromosomes were started as early as 1988[45] with an automatic algorithm included in the program IMAGIC. Semiautomatic programs for this purpose are now available, such as STERECON[71] and TINKERBELL[72] and in the framework of IMOD.[66]

A new exciting method (SITUS) (a public domain program),[73] available for testing, combines protein data from high resolution X-ray crystallography, available from the Protein Data Bank, with 3-D reconstructions with ETM. The program, which makes use of neural nets, searches the known protein configuration, as 'fingerprints', in the volume and, if found, displays its localization and orientation. This method would yield an identification method for proteins, without immunological techniques, and reveal their structure in the ETM-created volume at atomic resolution.

ACKNOWLEDGMENTS

For acquainting me with the practice of electron tomography, in 1989, I thank Lisa Borland, Marin van Heel

and Professor E. Zeitler, Head, Fritz Haber Institute, Berlin. Initial tips on MEM and further instruction on tomography methods, from Docent Ulf Skoglund, his tomography group (Lars-Göran Öfverstedt and Hans Mehlin) and Professor B. Daneholt, Head, Department of Cell and Molecular Biology, Karolinska Institute, Stockholm, are gratefully acknowledged. The visit to Karolinska Institute in 1993 was supported by EMBO and Nordiska Ministerrådet. Financial support from the foundations Maud Kuistilan Säätiö and Oskar Öflunds Stiftelse is gratefully acknowledged. At CSC-Scientific Computing, Espoo, Finland, the professional skills of Juha Ruokolainen, in both programming efficiency and physical theories, have been indispensable. Jukka Heikkonen of the Laboratory of Computational Engineering and Jorma Laaksonen of the Laboratory of Computer and Information Science, Helsinki University of Technology, have cooperated in the development and refinement of programs. For working facilities, for advice and for comments on the manuscript I thank Professor Antti Vaheri, Head, and Professor Carl-Henrik von Bonsdorff, Haartman Institute, University of Helsinki. The manuscript was thoroughly discussed with and scrutinized by Kalevi Pusa, who made a number of useful suggestions.

ABBREVIATIONS AND ACRONYMS

AA	Acetic Acid
Ab	Antibody
AD	Air Drying
CAVE	Computer-aided Virtual Environment
CCD	Charge-coupled Device
CHO	Chinese Hamster Ovary
CPD	Critical-point Drying
DAPI	4′,6-Diamidino-2-phenylindole
EM	Electron Microscopy
EMISH	Electron Microscopy In Situ Hybridization
ETM	Electron Tomography Method
FD	Freeze-drying
$FddH_2O$	Filtered Double-distilled Water
FG	Fish Gelatin
FISH	Fluorescence In Situ Hybridization
FITC	Fluorescein Isothiocyanate
GA	Glutaraldehyde
GAM	Goat Anti-mouse
GAR	Goat Anti-rabbit
HC	10 mM HEPES, pH 7.4, 5 mM $CaCl_2$
HEPES	*N*-(2-hydroxyethyl)piperazine-*N*′-(2-ethanesulfonic acid)
HM	10 mM HEPES, pH 7.4, 5 mM $MgCl_2$
IEM	Immunoelectron Microscopy
IET	Immunoelectron Tomography
LM	Light Microscopy
MAR	Matrix-associated Region
MEM	Maximum Entropy Method
MM	Mounting Medium
NC	Sodium Cacodylate
NE	Nuclear Envelope
NPC	Nuclear Pore Complex
o/n	Overnight
OT	Osmium Tetraoxide
PL	Poly-L-lysine
RPT	Rapid Prototyping Technology
RR	Ruthenium Red
RS	Ringer Solution
RT	Room Temperature
SAR	Scaffold-associated Region
SC	Synaptonemal Complex
SDS/PAGE	Sodium Dodecyl Sulfate Polyacrylamide Gel Electrophoresis
SGI	Silicon Graphics Inc.
SMC	Structural Maintenance of Chromosomes
TA	Tannic Acid
TEM	Transmission Electron Microscopy
TXHS	0.05% Triton X-100, 30 mM HEPES, pH 7.4, 0.1–0.5 M NaCl, 20 mM KCl, 5 mM $MgCl_2$, 20 mM glycine, 0.02% NaN_3
UA	Uranyl Acetate
WBM	Weighted Back-projection Method
2-D	Two-dimensional
3-D	Three-dimensional

RELATED ARTICLES

Biomolecules Analysis **(Volume 1)**
Biomolecules Analysis: Introduction • Single Biomolecule Detection and Characterization

Clinical Chemistry **(Volume 2)**
Immunochemistry • Molecular Biological Analyses and Molecular Pathology in Clinical Chemistry

Nucleic Acids Structure and Mapping **(Volume 6)**
Nucleic Acids Structure and Mapping: Introduction • DNA Probes • DNA Structures of Biological Relevance, Studies of Unusual Sequences • Fluorescence In Situ Hybridization

Peptides and Proteins **(Volume 7)**
Protein–Oligonucleotide Interactions

REFERENCES

1. W. Waldeyer, 'Über Karyokinese und ihre Beziehung zu den Befruhtungsvorgängen', *Arch. Micr. Anat.*, **32**, 1–122 (1888).
2. J.D. Watson, F.H.C. Crick, 'A Study of Deoxyribose Nucleic Acid', *Nature (London)*, **171**, 737–738 (1953).
3. P. Pasero, S.M. Gasser, 'New System for Replication DNA *in Vitro*', *Curr. Opin. Cell Biol.*, **10**, 304–310 (1998).
4. C.L. Woodcock, 'The Organization of Chromosomes and Chromatin', in *Electron Tomography: Three-dimensional Imaging with the Transmission Electron Microscope*, ed. J. Frank, Plenum Press, New York, 313–357, 1992.
5. E.J. DuPraw, *DNA and Chromosomes*, Holt, Rinehart and Winston, New York, 1970.
6. C.P. Fussel, 'The Rabl Orientation: a Prelude to Synapsis', in *Meiosis*, ed. P.B. Moens, Academic Press, New York, 275–299, 1987.
7. W.F. Marshall, A. Straight, J.F. Marko, J. Swedlow, A. Dernburg, A. Belmont, A.W. Murray, D.A. Agard, J.W. Sedat, 'Interphase Chromosomes Undergo Constrained Diffusional Motion in Living Cells', *Curr. Biol.*, **7**, 930–939 (1997).
8. P. Engelhardt, K. Pusa, 'Nuclear Pore Complexes: ''Press-stud'' Elements of Chromosomes in Pairing and Control', *Nature New Biol.*, **240**, 163–166 (1972).
9. M.E. Dresser, 'The Synaptonemal Complex and Meiosis: an Immunocytochemical Approach', in *Meiosis*, ed. P.B. Moens, Academic Press, New York, 245–274, 1987.
10. S.M. Gasser, 'Chromosome Structure, Coiling Up Chromosomes, Dispatch', *Curr. Biol.*, **5**, 357–360 (1995).
11. K. Nasmyth, 'Separating Sister Chromatids', *Trends Biochem. Sci.*, **24**(3), 98–104 (1999).
12. K. Luger, A.W. Mäder, R.K. Richmond, D.F. Sargent, T.J. Richmond, 'Crystal Structure of the Nucleosome Core Particle at 2.8 Å Resolution', *Nature (London)*, **389**, 251–260 (1997).
13. H. Ris, 'Higher Order Structures in Chromosomes', in *Proceedings of 9th International Congress on Electron Microscopy*, Canadian Society for Electron Microscopy, Toronto, 545–556, Vol. 3, 1978.
14. J.O. Thomas, 'Histone H1: Location and Role', *Curr. Opin. Cell Biol.*, **11**, 312–317 (1999).
15. R.D. Drinkwater, P.J. Wilson, J.D. Skinner, L.A. Burgoune, 'Chromatin Structures: Dissecting Their Mixed Patterns in Nuclease Digests', *Nucleic Acids Res.*, **15**, 8087–8103 (1987).
16. P.R. Walker, M. Sikorska, 'Chromatin Structure. Evidence that the 30 nm Fiber is a Helical Coil with 12 Nucleosomes/Turn', *J. Biol. Chem.*, **262**, 12223–12227 (1987)
17. R.A. Horowitz, A.J. Koster, J. Waltz, C.L. Woodcock, 'Automated Electron Microscope Tomography of Frozen-hydrated Chromatin: the Irregular Three-dimensional Zigzag Architecture Persists in Compact, Isolated Fibers', *J. Struct. Biol.*, **120**, 353–362 (1997).
18. B. Rydberg, W.R. Holley, I.S. Mian, A. Chatterjee, 'Chromatin Conformation in Living Cells: Support for a Zig-zag Model of the 30 nm Chromatin Fiber', *J. Mol. Biol.*, **284**, 71–84 (1998).
19. S.M. Gasser, B.B. Amati, M.E. Cardenas, J.F.-X. Hofman, 'Studies on Scaffold Attachment Sites and their Relation to Genome Function', *Int. Rev. Cytol.*, **119**, 57–96 (1989).
20. M.M.S. Heck, 'Condensin, Cohesins, and Chromosome Architecture: How to Make and Break a Mitotic Chromosome', *Cell*, **91**, 5–8 (1997).
21. P. Engelhardt, U. Plagens, I.B. Zbarsky, L.S. Filatova, 'Granules 25–30 nm in Diameter: Basic Constituent of the Nuclear Matrix, Chromosome Scaffold, and Nuclear Envelope', *Proc. Natl. Acad. Sci. USA*, **79**, 6937–6940 (1982).
22. P. Engelhardt, 'Higher Order Structure of Eukaryotic Chromosomes – Scaffold Elements and DNA Folding', Doctoral Dissertation, University of Helsinki, 1988. ISBN 952-90032-1-8. URL: http://www.csc.fi/jpr/emt/engelhar/Doc/Diss.html
23. H. Zentgraf, W. Franke, 'Differences of Supranucleosomal Organization in Different Kinds of Chromatin: Cell Type-specific Globular Subunits Containing Different Numbers of Nucleosomes', *J. Cell Biol.*, **99**, 272–286 (1984).
24. I. Manton, 'The Spiral Structure of Chromosomes', *Biol. Rev.*, **25**, 496–508 (1950).
25. J.B. Rattner, C.C. Lin, 'Radial Loops and Helical Coils Coexist in Metaphase Chromosomes', *Cell*, **42**, 291–296 (1985).
26. O. Haapala, 'Metaphase and Chromosome Banding are Distinct Entities of Chromosome Substructure', *Hereditas*, **100**, 75–81 (1984).
27. E. Boy de la Tour, U.K. Laemmli, 'The Metaphase Scaffold is Helically Folded: Sister Chromatids Have Predominantly Opposite Helical Handedness', *Cell*, **55**, 937–944 (1988).
28. P. Engelhardt, J. Ruokolainen, A. Dolenc, 'Electron Tomography of Chromosomes and Viruses', *CSC News*, **6**(4), 14–20 (1994). URL: http://www.csc.fi/jpr/emt/engelhar/csc/CSC-94.html
29. B. Alberts, D. Bray, J. Lewis, M. Raff, K. Roberts, J.D. Watson, *Molecular Biology of The Cell*, Garland Publishing, New York, 1994.
30. A.S. Belmont, 'Large-scale Chromosome Structure', in *Genome Structure and Function from Chromosomes Characterization to Genes Technology*, ed. C. Nicolini, Kluwer, Dordrecht, 261–278, 1996.
31. P.R. Cook, 'Commentary a Chromomeric Model for Nuclear and Chromosome Structure', *J. Cell Sci.*, **108**, 2927–2935 (1995).
32. P. Hozak, A.M.-J. Sasseville, Y. Raymond, P.R. Cook, 'Lamin Proteins form an Internal Nucleoskeleton as Well as a Peripheral Lamina in Human Cells', *J. Cell Sci.*, **108**, 635–644 (1995).

33. J. Newport, H. Yan, 'Organization of DNA into Foci During Replication', *Curr. Opin. Cell Biol.*, **8**, 365–368 (1996).
34. L. Reimer, *Transmission Electron Microscopy, Physics of Image Formation and Microanalysis*, Spinger Series in Optical Sciences, Springer, Berlin, 1997.
35. S. Hovmöller, 'CRISP: Cristallographic Image Processing on a Personal Computer', *Ultramicroscopy*, **41**, 121–135 (1992).
36. J. Frank (ed.), *Electron Tomography: Three-dimensional Imaging with the Transmision Electron Microscopy*, Plenum Press, New York, 1992.
37. D.J. De Rosier, A. Klug, 'Reconstruction of Three Dimensional Structures from Electron Micrographs', *Nature (London)*, **217**, 130 (1968).
38. R. Hart, 'Electron Microscopy of Unstained Biological Material: The Polytropic Montage', *Science*, **159**, 1464–1467 (1968).
39. W. Hoppe, R. Langer, G. Knesch, C. Poppe, 'Protein-Kristallstrukturanalyse mit Elektronenstrahlen', *Naturwissenschaften*, **55**(7), 333–336 (1968).
40. I. Daberkow, A.J. Koster, H.R. Tietz, D. Typke, J. Walz, 'A System for Automated Electron Tomography using Philips CM Series Transmission Electron Microscopes', *Philips Electron Opt. Bull.*, **134**, 27–31 (1996).
41. U. Skoglund, L.-G. Öfverstedt, R.M. Burnett, G. Bricogne, 'Maximum-entropy Three-dimensional Reconstruction with Deconvolution of the Contrast Transfer Function: a Test Application with Adenovirus', *J. Struct. Biol.*, **117**, 173–188 (1996).
42. J. Frank, *Three-dimensional Electron Microscopy of Macromolecular Assemblies*, Academic Press, New York, 1996.
43. M.C. Lawrence, M.A. Jaffer, B.T. Sewell, 'The Application of the Maximum Entropy Method to Electron Microscopic Tomography', *Ultramicroscopy*, **31**, 285–302 (1978).
44. G. Harauz, L. Borland, G.F. Bahr, E. Zeitler, M. van Heel, 'Three Dimensional Reconstruction of a Human Metaphase Chromosome from Electron Micrographs', *Chromosoma*, **95**, 366–374 (1987).
45. L. Borland, G. Harauz, G. Bahr, M. van Heel, 'Packing of the 30 nm Chromatin Fiber in the Human Metaphase Chromosome', *Chromosoma*, **97**, 159–163 (1988).
46. A.J. Koster, D.A. Agard, 'Editorial: Electron Tomography Workshop', *J. Struct. Biol.*, **120**, 207–209 (1996).
47. P. Engelhardt, J. Ruokolainen, F. Zhao, O. Carpén, A. Vaheri, 'Immunoelecron Tomography (IET) using Maximum Entropy Method Reveals 1.4 nm Gold Conjugates in 3-D Reconstruction of MCF-7 Cell Microvilli', in *SCANDEM-98, Proceedings of the 50th Annual Meeting of the Scandinavian Society of Electron Microscopy*, Scandem, Espoo, Finland, 86–87, 1998. URL: http://www.csc.fi/jpr/emt/engelhar/IET/Scandem-98-WWW.html
48. C.V. Hanson, 'Techniques in Isolation and Fractionation of Eukaryotic Chromosomes', in *New Techniques in Biophysics and Cell Biology*, eds. R.H. Pain, B.J. Smith, John Wiley & Sons, New York, 243–283, 1975.
49. J. Mendelsohn, 'Studies of Isolated Mammalian Metaphase Chromosomes', in *The Cell Nucleus*, ed. H. Busch, Academic Press, New York, 123–147, Vol. II, 1974.
50. G.F. Bahr, 'Determination of the Dry Mass of Biological Objects by Quantitative EM', in *Micromethods in Molecular Biology*, ed. V. Neuhoff, Springer, Berlin, 257–284, 1973.
51. A.J. Solari, 'Structural Analysis of Meiotic Chromosomes and Synaptonemal Complex in Higher Verteberates', *Methods Cell Biol.*, **53**, 235–256 (1997).
52. B.F. McEwen, M. Marko, 'Three-dimensional Transmission Electron Microscopy and its Application to Mitosis Research', *Methods Cell Biol.*, **61**, 81–111 (1999).
53. O.L. Miller, Jr, A.H. Bakken, 'Morphological Studies of Transcription', in *Karolinska Symposia on Research Methods in Reproductive Endocrinology, 5th Symposium on Gene Transcription Reproductive Tissue*, Karolinksa Institute, Stockholm, 155–173, 1972.
54. P. Engelhardt, J. Ruokolainen, 'Electron Tomography of Acetic Acid Isolated Whole-mount Chromosomes and Chromosome Scaffolds Suggests a Chromatin–Scaffold–Fiber Complex', in *EUREM-11, Proceedings of the 11th European Congress on Electron Microscopy (Dublin, Ireland, 26–30 August, 1996), Biology*, CESM, Brussel, 32–33, Vol. 3, 1998. URL: http://www.csc.fi/jpr/emt/engelhar/EUREM-96.html
55. L. Wollweber, R. Stracke, U. Gothe, 'The use of Simple Method to Avoid Cell Shrinkage During SEM Preparation', *J. Microsc.*, **121**(2), 185–189 (1980).
56. H. Ris, 'The Cytoplasmic Filament System in Critical Point-dried Whole Mount and Plastic-embedded Sections', *J. Cell Biol.*, **100**, 1474–1487 (1985).
57. K.R. Porter, M.E. Stearns 'Stereomicroscopy of Whole Cells', *Methods Cell Biol.*, **22**, 53–75 (1981).
58. T. Inoué, H. Osatake, H. Takahashi, 'A New Freeze-drying Instrument using t-Butyl Alcohol for Scanning Electron Microscopy', *J. Electron Microsc.*, **38**(4), 246–249 (1989).
59. J. Heuser, 'Preparing Biological Samples for Stereomicroscopy by the Quick-freeze, Deep-etch, Rotary-replication Technique', *Methods Cell Biol.*, **22**, 97–122 (1981).
60. M.V. Nermut, A.C. Steven (eds.), *Animal Virus Structure*, Elsevier, Amsterdam, 1987.
61. M.A. Hayat, *Negative Staining*, McGraw-Hill, New York, 1990.
62. M.W. Clark, 'Immunogold Labeling of Yeast Ultrathin Sections, Appendix B', *Methods Enzymol.*, **194**, 608–626 (1991).
63. S. Penman, 'Rethinking Cell Structure', *Proc. Natl. Acad. Sci. USA*, **92**, 5251–5257 (1997).
64. J.N. Turner, U. Valdrè, 'Tilting Stages for Biological Applications', in *Electron Tomography: Three-dimensional Imaging with the Transmission Electron*

Microscope, ed. J. Frank, Plenum Press, New York, 167–194, 1992.
65. *Model 630 High Tilt Cryotransfer*, Gatan Inc., Pleasanton, CA. URL: http://www.gatan.com
66. J.R. Kremer, D.N. Mastronarde, J.R. MacIntosh, 'Computer Visualization of Three-dimensional Image Data using IMOD', *J. Struct. Biol.*, **116**, 71–76 (1996).
67. G. Grifiths, *Fine Structure Immunochemistry*, Spinger, Berlin, 1995.
68. J. Ruokolainen, P. Engelhardt, 'Maximum-entropy an Electron-tomography Program Kit for Silicon Graphics Computers', in *3-D Imaging Sciences in Microscopy, 15–17 April, Conference Proceedings*, Royal Microscopical Society, London, 1996.
69. P. Penczek, M. Marko, K. Buttle, J. Frank, 'Double-tilt Electron Tomography', *Ultramicroscopy*, **60**, 393–410 (1995).
70. D.N. Mastronarde, 'Dual-axis Tomography: an Approach with Alignment Methods that Preserve Resolution', *J. Struct. Biol.*, **120**, 343–352 (1997).
71. M. Marko, A. Leith, 'Sterecon – Three-dimensional Reconstruction from Stereoscopic Contouring', *J. Struct. Biol.*, **116**, 93–98 (1996).
72. Y.-H. Li, A. Leith, J. Frank, 'Tinkerbell – A Tool for Interactive Segmentation of 3-D Data', *J. Struct. Biol.*, **120**, 266–275 (1997).
73. W. Wriggers, R.A. Milligan, J.A. McCammon, 'Situs: a Package for Docking Crystal Structures into Low-resolution Maps from Electron Microscopy', *J. Struct. Biol.*, **125**, 185–195 (1999).